Modeling Subcloud Layer Structure and Interaction with a Shallow Cumulus Layer

ALAN K. BETTS

Department of Atmospheric Science, Colorado State University, Fort Collins 80523

(Manuscript received 16 March 1976, in revised form 26 August 1976)

ABSTRACT

This paper couples a mixed subcloud layer model developed by several authors with the cumulus flux parameterization proposed by Betts (1975). Cloud base mass flux and mass flux gradient are related to subcloud layer parameters and cumulus layer gradients using two parameters, α and β. The α symbol is the ratio of a *model* transition layer depth to the subcloud layer depth, and β is the ratio of a *model* cloud base static energy flux to the surface flux. For the simple case of a steady-state transition layer, the subcloud layer heat and moisture budgets are predicted.

Data from a field experiment over Venezuela are used to illustrate mean subcloud layer structure and to derive heat and moisture flux profiles and model parameters from a simple budget analysis. The data give $(\alpha,\beta) = (0.11, 0.41)$ and correspondingly, $(\alpha_v,\beta_v) = (0.08, 0.21)$ based on virtual static energy fluxes and profiles. During the budget time period (centered on local noon over land) the subcloud layer warms and dries with a corresponding rise of cloud base. The steady-state transition layer model predictions showed qualitative agreement with the fluxes derived from the budget. The extension of the convective mass flux model into the subcloud layer was shown to be feasible. It illustrates the rapid decrease of convective mass flux across the transition layer.

The paper concludes that the model is a satisfactory diagnostic tool for subcloud layer budgets and the cloud-subcloud layer interaction, and may have predictive value.

1. Introduction

This paper is concerned with a model for the thermodynamic structure of the nearly well-mixed subcloud layer and with its interaction with an overlying shallow cumulus layer. Early mixed layer models were presented by Ball (1960) for dry convection, Kraus and Turner (1967) for the mixed ocean thermoline and Lilly (1968) for stratocumulus. Deardorff *et al.* (1969) presented an observational study. Subsequently, Betts (1973), Carson (1973) aud Tennekes (1973) all proposed very similar models for a mixed layer of dry convection. Stull (1973) discussed the mixed layer development in terms of a penetrative convection model. Betts (1973) also presented a mixed sublcoud layer model. There has been considerable subsequent discussion of these models (Deardorff *et al.*, 1974; Betts, 1974; Zilitinkevich, 1975; Tennekes, 1975) as well as laboratory simulations (Willis and Deardorff, 1974) and three-dimensional numerical simulations of an inversion capped mixed layer Deardorff (1974a,b). Several tropical parameterization and budget studies have used the mixed subcloud layer model: Arakawa and Schubert (1974), Sarachik (1974), Ogura and Cho (1974), and the testing of this model was proposed for the Boundary Layer Subprogramme for GATE (Hoeber, 1973). However, several authors (Sarachik, 1974; Esbensen, 1975; Lemone and Pennell, 1976) have suggested that the interaction between the cumulus layer and the subcloud layer is not well described by present models. Betts (1975) pointed out that the convective heating at cloud base cannot be parameterized solely in terms of a vertical mass flux, which was an assumption in Betts (1973). The purpose of this paper is to couple the mixed layer model to the cumulus parameterization of Betts (1975) to give a more general model for the cloud-subcloud interaction, and to illustrate it using data for the structure and time-change of the subcloud layer over land.

The subcloud layer model is a thermodynamic mixed layer model, in which air rises from the mixed subcloud layer to form clouds while the environment subsides uniformly between the clouds. No precipitation is assumed. Betts (1976) has presented a second model for the situation where the cloud-subcloud interaction is dominated by precipitation and downdrafts as well as updrafts. Some preliminary results for the structure of the subcloud layer were presented in Dugan (1973) and Betts *et al.* (1974). In this paper we shall initially present observational evidence for the mixed subcloud layer structure, then develop the model and compare the model with the mean change in the subcloud layer for the 1000–1400 (local) time period. The convective mass transport model will also be applied to the subcloud layer to illustrate the decrease in convective

mass flux across cloud base. Finally, some unresolved questions concerning subcloud layer structure will be discussed.

Although the model will here be tested diagnostically using tropical land data, it is hoped that it will have wider applicability to the modeling of the cloud-subcloud interaction in undisturbed convective regimes including the tropical ocean studied during the GARP Atlantic Tropical Experiment.

2. Experiment and data processing

The data were collected during the second Venezuelan International Meteorological and Hydrological Experiment (VIMHEX-1972), conducted in north-central Venezuela during the summer rainy season of 1972. A major objective of the experiment was the study of tropical convection with a view towards developing parametric models. The experimental design was very simple. A 10 cm calibrated radar (an extensively modified M-33 radar) and a GMD-1 rawinsonde unit were located at Carrizal, Venezuela (9°22.8′N, 66°55.0′W) within a raingage network of diameter 120 km. The experiment's resources were limited, and the main emphasis was on the study of precipitating convection. Sequences of soundings were launched whenever significant radar activity was observed. Nonetheless, half the days had little precipitation, and many soundings were made in an undisturbed convective regime with the sky typically covered with a few tenths shallow cumulus; these data, used in this paper, consist of soundings taken in the absence of precipitation. Typically, a characteristic nearly well-mixed thermodynamic structure was observed in the subcloud layer.

Temperature and relative humidity were computed from strip chart values at every baroswitch contact point (where the sonde switches from the temperature to the humidity sensor) from the surface to about 650 mb. At these low levels, baroswitch contact points are spaced at about 10 mb intervals at known pressures. Humidity values are missing every fifth contact point where a reference signal is sampled: these humidities were interpolated linearly from the adjacent values. The temperature and humidity data were corrected for the thermal lags of both the thermistor and hydristor (see Appendix A). These corrections are small ($\Delta T \approx -0.2$°C, $\Delta q \approx 0.5$ g kg^{-1}) for the VIZ 1290 series radiosonde used in the experiment, but are significant in this study because both corrections lower the height of the lifting condensation levels of air in the subcloud layer which were used to estimate cloud-base (see below). Specific humidity, hydrostatic height and the lifting condensation level pressure (LCLP) were computed for each data level.

In this paper we present only average profiles. These reflect very well the typical vertical structure of individual soundings while showing less noise. (The basic data uncorrected for sensor lags and at 10 mb levels are available from the author in Betts and Miller, 1975.) Before averaging, the pressure levels of each sounding were scaled by the pressure depth of the subcloud layer to give a dimensionless pressure

$$\hat{p}=\frac{p_0-p}{p_0-p_B},$$

where p_B is cloud-base pressure, and p_0 the surface pressure, which varied only a little from 990 mb. In these scaled coordinates, the surface becomes $\hat{p}=0$ and cloud-base 1.0. Cloud-base pressure p_B was taken as the *average* pressure of the LCLP's for all data levels in the subcloud layer. Fig. 1 shows that this value of p_B can be regarded also as a mixed layer average LCLP.

After scaling, as above, data values were interpolated to increments in $\hat{p}$ of 0.05 from $\hat{p}=0$ to $\hat{p}=1.5$ before averaging. In this paper, we shall use static energies since they are additive functions. The dry static energy is

$$s=C_pT+gz,$$

where z is the hydrostatic height, C_p the specific heat at constant pressure (taken constant as 1.005×10^3 J kg^{-1}). The moist static energy is

$$h=s+Lq,$$

where q is the specific humidity, and L the latent heat of vaporization was taken as 2474×10^3 J kg^{-1}). For saturated air with no fallout of liquid water, these become the liquid water static energy (Betts, 1975)

$$s_l=s-Lq_l,$$

where q_l is the parcel liquid water content, and the saturation static energy

$$h_s=s+Lq_s,$$

where q_s is the saturation specific humidity.

The surface data were measured using an aspirated psychrometer in the shade at the launch site. However, the launch site, located near the edge of an unused airfield, may not be very representative of the surrounding brush and grassland. Some sample comparison surface observations indicated that the launch site was a little warmer and drier, but no systematic comparison was made. Fig. 1 indicates a smaller fall in the specific humidity (as Lq) just above the surface in comparison with the fall of s. This also suggests some systematic bias in the surface values (too warm and too dry), although the humidity data could have been over-corrected (see Appendix A).

3. Subcloud layer structure

a. *Mean profile*

Fig. 1 shows a scaled average of 135 soundings. This comprises most of the VIMHEX 1972 soundings taken

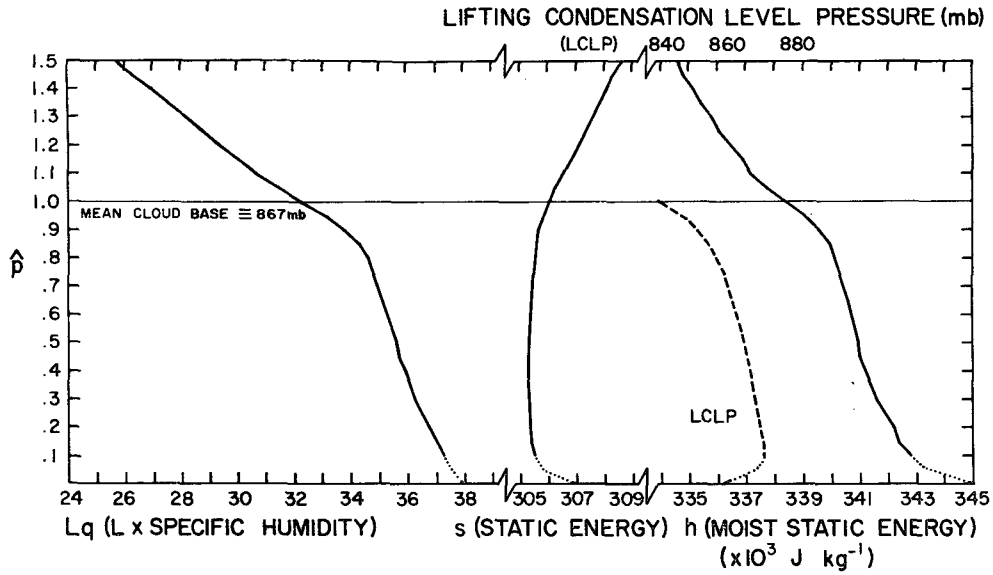

FIG. 1. Average of 135 soundings associated with nonprecipitating convection showing profiles of latent energy, static energy, moist static energy (solid profiles) and pressure of the lifting condensation level (dashed profile). The profiles are dotted below $\hat{p}=0.1$ because the surface data may not be representative. The mean surface pressure is 992 mb.

on days without significant precipitation or before the onset of showers on other days. A few soundings with processing problems or suspect data have been eliminated. The cloud base estimate used for scaling each sounding was the mean LCL in the subcloud layer.

The mean profile shows several significant features. The static energy (and also potential temperature) shows a minimum at $\hat{p}=0.40$; thus a weak superadiabatic layer extends well above the strong surface superadiabatic layer below, say, $\hat{p}=0.10$. The upper part of the subcloud layer is stable, becoming more so at $\hat{p}=0.9$ and in the cumulus layer. Mixing ratio falls steadily from $\hat{p}=0.1$ to 0.85 and more sharply above $\hat{p}=0.85$. The LCLP profile shows a maximum just above the surface layer at $\hat{p}=0.15$, falls slowly with height to $\hat{p}=0.85$ and then more steeply. As mentioned in the previous section, the surface data may be subject to systematic bias (indicated by the dotted profiles below 0.1) so that the decrease of LCLP below $\hat{p}=0.10$ may be spurious.

b. *Mean time change*

Fig. 2 shows the time change from 1000 local time to 1400. Each curve is an average of twenty soundings for the twenty days on which soundings were taken at 1000 and 1400 and no precipitation fell between these times. The profiles are similar to Fig. 1 in vertical structure. In this 4 h period centered on local noon, the subcloud layer warms about 3.7×10^3 J kg^{-1} (equivalent to about 4 K), and dries a similar amount with little change in mean moist static energy. Cloud base lifts about 70 mb. These changes are typical of the daily pattern of convection.

Both the vertical gradients and absolute differences of h and Lq across the mixed layer increase from 1000 to 1400. The s profile shows little change. Other mean soundings also show some indication of a steepening of the water vapor gradient during the day in the subcloud layer as the layer dries out. The mean change shown in Fig. 2 will be used in Section 5 to derive convective fluxes from the surface to $\hat{p}=1.5$ and to test diagnostically the model developed in Section 4.

c. *The transition layer and ascents into cloud*

Neither Fig. 1 nor 2 show a significant "transition layer." That is, one cannot find a marked stable layer near cloud base in the average. Although many soundings show a stabilization between two contact levels near cloud base, not all do, nor is this stabilization always at the same level relative to cloud base. To illustrate the transition layer in an average is difficult unless soundings are scaled by a transition layer base selected by eye. This we shall not do. We shall, however, illustrate the stabilization near cloud base in soundings which ascend between clouds by presenting average profiles for 19 soundings which were observed to enter cloud base and 20 soundings which were either observed to pass between clouds, or for which no visual observation was available. All soundings were taken at about 1000 local time, which means all are for different days. Fig. 3 shows the mean profiles. Each sounding was scaled by its mean sublcoud layer LCLP before the average was generated as in Figs. 1 and 2. The "transition layer" set (heavy line) was selected from the larger set of 1000 ascents which were not observed to pass through cloud base by selecting soundings with

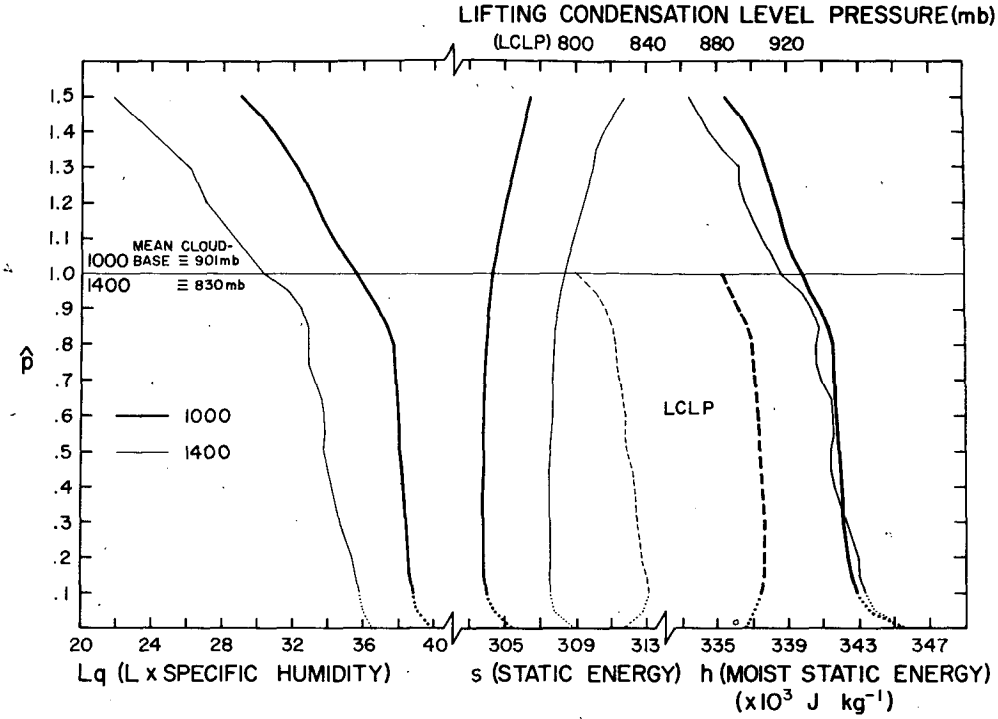

FIG. 2. Average profiles (as Fig. 1) for 1000 (heavy lines) and 1400 (light lines) soundings (local time) from 20 days of nonprecipitating convection, showing warming and drying of the subcloud layer. The mean surface pressure is 994 mb at 1000 and 990 mb at 1400.

mean subcloud layer LCL between 896 and 923 mb. This gave a mean LCLP for the 20 sounding average of 910 mb, the *same* as the "into cloud" average. Thus, although the soundings in Fig. 3 are averages for different days, they have the same average cloud base and can be qualitatively compared. The "into cloud"

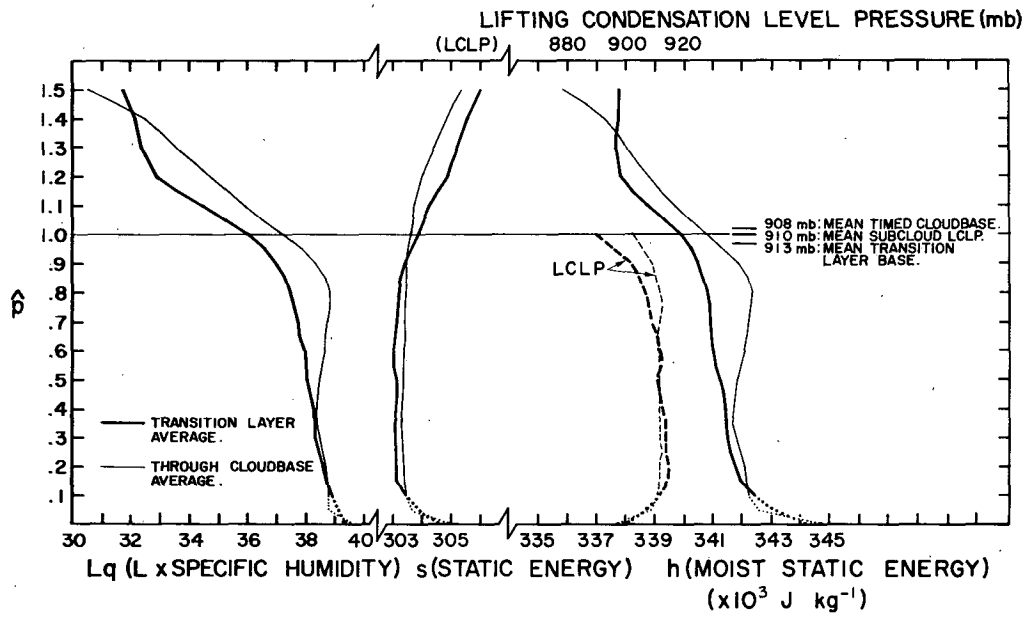

FIG. 3. Average profiles (as Fig. 1) for 19 soundings which entered cloud-base (light lines) and 20 soundings which probably passed between clouds (heavy lines). All soundings were launched near 1000 local time; the mean surface pressue is 994 mb for both. The fall in Lq, h and LCLP just below cloud-base is believed to be instrumental for the "through cloud-base" average.

average is warmer and moister below cloud base and more "well mixed" than the "transition layer" average. The fall of mixing ratio between $0.85<\hat{p}<1.0$ is probably instrumental (the relative humidity reaches 95% at $\hat{p}=0.85$). The transition layer case shows a marked stabilization starting below cloud base where the s profiles cross, and an earlier fall of mixing ratio. The subcloud LCLP profile of the "transition layer" case resembles those of Figs. 1 and 2. Above cloud base, the "into cloud" soundings are cooler. Although there is no information on how long the balloon remained within a cloud, and no assurance that the difference between the independent averages accurately represents cloud-environment differences, the figure suggests that, even with the virtual temperature correction, small cumulus clouds must be negatively buoyant at cloud base, and probably no more than marginally buoyant above.

In Fig. 3, $\hat{p}=1.0$ corresponds to a subcloud mean LCL of 910 mb for both averages. The ascent time of balloons which were observed to disappear through cloud base was measured and a cloud base pressure was found from the corresponding time on the strip chart. For each sounding the difference between subcloud layer mean LCLP (p_{LCL}) and the timed cloud base (p_B) was found. The mean value for the sample of 19 was

$$\overline{(p_{LCL}-p_B)}=2\pm6 \text{ mb},$$

corresponding to an average *timed* cloud base of 908 mb. This suggests that the mean LCL of the subcloud layer is a good estimate of cloud base. Betts *et al.* (1974) presented a similar but preliminary analysis based on uncorrected data (see Appendix A).

For the transition layer average, the *base* of the transition layer (p_{TLB}) was estimated from the contact level data as the level above which the static energy (and potential temperature), which are nearly constant in the mixed layer, took a marked jump. Two of the twenty soundings showed no discernible jump but only a smooth change of stratification from the mixed subcloud layer to the cumulus layer. For the remainder, the difference $p_{LCL}-p_{TLB}$ was tabulated. The mean value was

$$\overline{(p_{LCL}-p_{TLB})}=-3\pm6 \text{ mb}.$$

That is, the transition layer base averaged 913 mb. It appears the transition layer base is a little below cloud base in the mean. However, the spread of $(p_{LCL}-p_{TLB})$ leads to a smoothing out of the transition layer in Fig. 3. The thickness of the transition layer is not well resolved in this data since contact level data points are spaced about 10 mb apart.

d. General features

The mean profiles presented in this section show several common features:

1) A strong surface superadiabatic layer $0<\hat{p}<0.15$.

2) A near neutral s layer between $0.15\leqslant\hat{p}\leqslant0.85$ with a minimum of s at $\hat{p}\approx0.4$: that is, s decreasing up to 0.4 and increasing above.

3) An increase in the s gradient for $\hat{p}\gtrsim0.9$.

4) A steady fall of q above the superadiabatic layer to $\hat{p}=0.85$ and a steeper fall for $\hat{p}>0.85$.

5) The lifting condensation pressure of air in the subcloud layer falls slowly above the surface superadiabatic layer.

One could distinguish a mixed layer to $\hat{p}=0.85$ as distinct from the subcloud layer up to $\hat{p}=1.0$, although even below $\hat{p}=0.85$ the specific humidity falls with height. Mixed layer models ignore this vertical variation. In the model presented in the next section, the entire layer $0<\hat{p}<1.0$ below cloud base will be treated as a "mixed" layer, rather than attempt to distinguish between a "mixed" layer and the subcloud layer. In Section 5e, the subcloud layer fluxes and profiles and the limitations of the mixed layer model will be discussed briefly.

4. Model for cloud-subcloud interaction

In a dry convective layer capped by an inversion, the inversion rise is controlled by the so-called "entrainment" of the warmer air above the inversion into the highly turbulent convective layer. There is a convergence of turbulent kinetic energy, generated by buoyancy in the nearly well mixed layer, into the inversion layer, and an associated downward heat flux. The entrainment of air above requires that this air both be cooled to the mixed layer potential temperature and be supplied with the same turbulent energy level (e.g., Zilitinkevich, 1975).

Below a cumulus layer, this same process operates, but the subcloud layer is capped by a rather weak, stable layer, usually called the transition layer. The transition layer is located at or just below cloud base or the condensation level of rising convective elements. Now, however, a certain fraction of the subcloud convective elements rise through the transition layer into the stable cumulus layer above, where they of course form clouds. The depth of the mixed layer is now dictated not by a simple deepening process but by some relation to the height of cloud base. There is also now a convective mass flux out of the subcloud layer associated with the formation of clouds. In addition, budget studies (Nitta and Esbensen, 1974; Betts, 1975) have shown that the cloud convective mass flux is rapidly changing near cloud base, implying a large detrainment of "cloud-mass" at this level. The distinction between detrainment of cloud mass flux and of subcloud layer dry convective elements is indeed a largely artificial construct divided only by the lifting condensation level which may itself vary somewhat from convective element to element. Nonetheless, a large detrainment (with an associated cooling) of convective elements is

taking place near cloud base. This cooling of the inversion layer by the *detrainment* of convective elements is the same process referred to above as the *entrainment* of air from the inversion layer into the well-mixed layer.

However, it is still useful to identify cloud base in a model, where the phase change of water becomes important, and it proves necessary to define both a cloud-base mass-flux (ω_B^*) out of the mixed layer and a mass flux gradient at cloud base. Deardorff (1970b) has defined a convective velocity scale (which we here symbolize Ω_*—see Section 4f) related to the surface heat flux. With an overlying cumulus layer the convective fluxes do not go to zero just above the mixed layer. Just as Ω_* is related to the surface flux, so ω_B^* is related to the cloud base flux. In Section 4f, we shall nondimensionalize the cloud-subcloud layer equations using the convective velocity scale, subcloud layer depth and related scales for static energy and latent energy (Lq).

In this section, the subcloud layer will be treated simply as a "well-mixed" layer by using vertically averaged static energy and water vapor. (An extension of the convective mass flux model into the subcloud layer will be attempted later in Section 5e using observed profiles.)

The following analysis draws on many papers already cited (Betts, 1973, 1974, 1975; Carson, 1973; Deardorff, 1974; Tennekes, 1973; Zilitinkevich, 1975). The primary extensions are to express the "jump" in Δs at the top of the subcloud layer in terms of a parameter Δp (which may be regarded as the thickness of a *model* transition layer) and to incorporate a cloud base mass flux which changes rapidly near cloud base. The individual equations and the solution of the system of equations for the case of a steady-state transition layer will be compared with a simple budget study in Section 5.

a. Subcloud layer budget

The simplified budget equation, which neglects large-scale horizontal gradients of s and horizontal eddy transports, as well as large-scale storage and advection of liquid water, is (Betts, 1975)

$$\frac{\partial \bar{s}}{\partial t}+\tilde{\omega}\frac{\partial \bar{s}}{\partial p}=R-\frac{\partial}{\partial p}(\widetilde{\omega' s_l'}), \tag{1}$$

where the tilde denotes a large-scale horizontal average, R is the radiative source term and s_l is the liquid water static energy. Below cloud base, $s_l=s$, but because there is some uncertainty as to the level of cloud base it is preferable to retain the generality. Further, we shall use (1) integrated to an arbitrary level for the budget analysis in Section 5.

Assuming that $\partial\tilde{\omega}/\partial p$ is independent of pressure (for simplicity) and defining an average from the surface p_0 to cloud base p_B by an overbar

$$(p_B-p_0)\bar{\tilde{x}}=\int_{p_0}^{p_B}\tilde{x}\,dp,$$

Eq. (1) can be integrated to

$$(p_B-p_0)\frac{d\bar{\tilde{s}}}{dt}+\left(\frac{dp_B}{dt}-\tilde{\omega}_B\right)(\bar{\tilde{s}}-\tilde{s}_B)$$

$$=(\widetilde{\omega' s'})_0-(\widetilde{\omega' s_l'})_B+\bar{\tilde{R}}(p_B-p_0), \tag{2}$$

where we have assumed $\partial p_0/\partial t=0$ and $\tilde{\omega}_0=0$. The subscript l will be superfluous provided all clouds have their condensation levels at or above the chosen level B.

We define a subcloud layer thickness

$$P=p_0-p_B;$$

thus,

$$\frac{dP}{dt}=-dp_B/dt$$

if the surface pressure is constant. We then define the strength of the transition layer

$$\Delta s=\tilde{s}_B-\bar{\tilde{s}}, \tag{3}$$

a surface flux

$$F_{0s}=-\widetilde{\omega' s_0'},$$

and a convective mass flux ω^* (Betts, 1975) so that

$$F_{Bs_l}=-(\widetilde{\omega' s_l'})_B=\omega_B^*(s_{lc}-\bar{\tilde{s}})_B. \tag{4}$$

The suffix denotes a representative value for a convective element (cloud above cloud base). To construct a simple *mixed* layer model it will be assumed that air rising to form clouds will have mixed layer properties: $s_{lc}=\bar{\tilde{s}}$ at cloud base. Then (4) becomes

$$F_{Bs_l}=-\omega_B^*\Delta s. \tag{5}$$

This is a negative flux: Δs and ω_B^* have been defined to be positive for the typical case (see Section 5).

With these simplifications, Eq. (2) can be rewritten as

$$P\frac{d\bar{\tilde{s}}}{dt}=F_{0s}+\left(\frac{dP}{dt}+\tilde{\omega}_B+\omega_B^*\right)\Delta s+P\bar{\tilde{R}}. \tag{6}$$

This equation describes the warming of the mean subcloud layer. It is heated by the surface flux F_{0s}, by the deepening of the layer dP/dt or by subsidence ($\tilde{\omega}$ positive) which incorporates warmer air ($\tilde{s}_B>\bar{\tilde{s}}$) into it, and also heated by cumulus convection, parameterized here as $\omega_B^*\Delta s$. The radiative term will typically be a cooling term. This equation was used (without radiation) in Betts (1973).

b. Cloud base heating rate and the transition layer

The time rate of change of $\bar{s}$ just *above* cloud base ($d\bar{s}_B/dt$) will be expressed using the parameterization of the cumulus convection proposed in Betts (1975); $d\bar{s}_B/dt$ includes the effect of rising cloud base, as well as cumulus heating and large-scale vertical advection:

$$\frac{d\bar{s}_B}{dt}=-\left(\frac{dP}{dt}+\tilde{\omega}_B+\omega^*_B\right)\left(\frac{\partial\bar{s}}{\partial p}\right)_B+\left(\frac{\partial\omega^*}{\partial p}\right)_B(s_{lc}-\bar{s})_B+R_B. \quad (7)$$

The formulation neglects entrainment into clouds at cloud base. At cloud base, the definition of Δs gives

$$(s_{lc}-\bar{s})_B=\bar{\bar{s}}-\bar{s}_B=-\Delta s$$

and a further definition of the stratification just above cloud base

$$\Gamma_s=-\left(\frac{\partial\bar{s}}{\partial p}\right)_B$$

can be used, giving

$$\frac{d\bar{s}_B}{dt}=\left(\frac{dP}{dt}+\tilde{\omega}_B+\omega^*_B\right)\Gamma_s-\left(\frac{\partial\omega^*}{\partial p}\right)_B\Delta s+R_B. \quad (8)$$

Typically, the first term in (8) is a warming term, and the second a cooling term associated with the detrainment (ω^* decreasing with height) of "cooler" clouds ($s_{lc}<\bar{s}$).

A basic problem with this parameterization is that ω^* is rapidly decreasing with height near cloud base (see Ogura and Cho, 1973; Yanai *et al.*, 1973; Nitta, 1975; Betts, 1975). $\partial\omega^*/\partial p$ is correspondingly large, while $\Delta s=(\bar{s}-s_{lc})$ is very small; yet the convective flux and flux gradient are well defined and in diagnostic studies change smoothly. One of the aims of this paper is to avoid these difficulties by expressing the convective fluxes and flux divergences in terms of cloud base parameters.

We shall define a *model* parameter Δp by projecting the stratification just above cloud base back onto the model mixed layer, so that

$$\Delta p=\Delta s/\Gamma_s. \quad (9)$$

This could be regarded as the layer of convective overshoot at the top of the dry convective layer (see Carson, 1973), or as approximately the layer between the top of the "mixed" layer and cloud base, as in Arakawa and Schubert (1974). We shall regard Eq. (9) as a definition of a *model transition layer* thickness. A value for Δp will be found diagnostically from mean profiles (Fig. 2). This "overshoot" layer is clearly a layer of critical importance to the control of the cumulus convection and, consequently, the cloud-subcloud interaction (Betts, 1973).

Formally, we may multiply (8) by Δp and define a cloud base detrainment $\Delta\omega^*_B$,

$$\Delta\omega^*_B=(\partial\omega^*/\partial p)_B\Delta p, \quad (10)$$

giving

$$\Delta p\frac{d\bar{s}_B}{dt}=\left(\frac{dP}{dt}+\tilde{\omega}_B+\omega^*_B-\Delta\omega^*_B\right)\Delta s+R_B\Delta p. \quad (11)$$

The subcloud layer s budget will be solved using this equation, Eq. (6) and a closure equation [(13a)] (see Section 4d). Note that (11) contains two parameters for the cumulus convection: a convective mass flux at cloud base and one related to the mass-flux gradient.

Eq. (11) was derived from the heating rate above cloud base, but it is related in the case of a steady-state model transition layer (Δs, Δp constant) to the transition layer budget (see Appendix B).

c. Closure

In papers previously cited (Betts, 1973; Carson, 1973; Tennekes, 1973) the mixed layer model was closed by relating the heat flux (F_{s-}) at the base of the capping model inversion to the surface heat flux, using a turbulent kinetic energy budget for the mixed layer giving

$$F_{s-}=-\beta F_{0s}. \quad (12)$$

Values of β in the range 0.2 to 0.5 have been suggested. Zilitinkevich (1975) has extended the model to include the turbulent kinetic energy budget of the inversion itself, and found that as the inversion strength increases, β increases. Carson (1973) estimated near maximum heating that β was as large as 0.5. The case of an inversion capping a dry convection layer is simplified by the fact that above the inversion, $F_s=0$.

For the subcloud layer, the inversion strength Δs is relatively weak, but the budget studies in Section 5 indicate a relatively large value of F_s/F_{0s} near cloud base.

What is unclear in the case of the cloud-subcloud layer interaction is what is the appropriate F_{s-}. The derived static energy flux F_s becomes larger negative up to cloud base (see Figs. 4 and 8) and, as F_{sl}, continues to increase in magnitude above cloud base. At what level should F_s be compared to F_{0s}? An analysis too of a transition layer turbulent kinetic energy budget which partitions the turbulence into a cloud fraction and a subcloud fraction is clearly necessary. The kinetic energy of the cloud fraction is coupled through the perturbation pressure field to the clouds above, but is probably of less importance to the maintenance of the transition layer than the kinetic energy budget of the "trapped" subcloud layer turbulence. A theoretical model for this closure will not be attempted in this paper. Instead, a budget study will be used to indicate an observational value of β.

Two possibilities for closure are discussed in more detail in Appendix B. The one we shall use to close the

system is

$$-\left(\frac{dP}{dt}+\tilde{\omega}_B+\omega_B^*\right)\Delta s=-\beta F_{0s}. \tag{13a}$$

This goes over uniformly into the familiar dry mixed layer model as the cumulus component goes to zero, namely (*loc. cit.*)

$$F_{s-}=-\left(\frac{dP}{dt}+\tilde{\omega}_B\right)\Delta s=-\beta F_{0s}. \tag{14}$$

This component of F_{s-} as noted by Deardorff *et al.* (1974) is largely a construct of the averaging to give a mixed layer [see derivation of Eq. (3)]. Whenever a mixed layer is constructed, a term of this type will appear, and closure using (13a) simplifies the problem greatly. Closure (13a) will formally be used here to avoid inconsistency with the no cloud case. It greatly simplifies Eqs. (6) and (11).

For a moist system, buoyant kinetic energy generation is related to the virtual static energy flux. However, since the theoretical validity of the closure is unclear, we shall preserve the simplicity of the separate s and Lq budgets in this diagnostic study. From these, one can derive virtual static energy parameters and fluxes and a corresponding β_v. The s_v equations are entirely analogous to the s equations.

d. System of s equations

A summary of the system of s equations for the subcloud layer is presented:

$$P\frac{d\bar{\bar{s}}}{st}=F_{0s}+\left(\frac{dP}{dt}+\tilde{\omega}_B+\omega_B^*\right)\Delta s+P\bar{\bar{R}} \tag{6}$$

$$\Delta p\frac{d\tilde{s}_B}{dt}=\left(\frac{dP}{dt}+\tilde{\omega}_B+\omega_B^*-\Delta\omega_B^*\right)\Delta s+\Delta p R_B \tag{11}$$

$$\Delta s=\tilde{s}_B-\bar{\bar{s}} \tag{3}$$

$$\Delta s=\Gamma_s\Delta p \tag{9}$$

$$\beta F_{0s}=\left(\frac{dP}{dt}+\tilde{\omega}_B+\omega_B^*\right)\Delta s. \tag{13a}$$

If $P(t)$ and Δp are known as well as β, F_{0s}, R, $\tilde{\omega}$ and Γ_s, there are five equations which can be solved for the five remaining variables $\bar{\bar{s}}$, $\tilde{s}_B$, Δs, ω_B^* and $\Delta\omega_B^*$. $P(t)$, cloud base, can be found from the mixed layer condensation level from $\bar{\bar{s}}(t)$ and $\bar{\bar{q}}(t)$ (Eq. 16) using Eq. 19 (see below). In this paper we shall take the approach of *specifying* Δp through the relation

$$\Delta p=\alpha P, \tag{15}$$

so that ω_B^* and $\Delta\omega_B^*$ can be found from the subcloud layer time dependence. A characteristic value of α can be found from the mean profiles (Figs. 1 and 2). It should be noted, however, that the equations above are only a small subset of the heat and moisture equations for the whole coupled cloud-subcloud system which simultaneously determines ω_B^*, $\Delta\omega_B^*$ and Δp. Δp corresponds to the variable difference in height between cloud base and mixed layer top (Z_c-Z_B) in Arakawa and Schubert (1974), who have proposed a method of solution for the whole system.

e. System of q equations

The water substance equations corresponding to Section 4d are close analogs and will not be derived, except to note that $\Delta q\neq\Gamma_q\Delta p$ as in Eq. (9):

$$P\frac{d\bar{\bar{q}}}{dt}=F_{0q}+\left(\frac{dP}{dt}+\tilde{\omega}_B+\omega_B^*\right)\Delta q \tag{16}$$

$$\Delta p\frac{d\tilde{q}_B}{dt}=\left(\frac{dP}{dt}+\tilde{\omega}_B+\omega_B^*\right)\Gamma_q\Delta p-\Delta\omega_B^*\Delta q \tag{17}$$

$$\Delta q=\tilde{q}_B-\bar{\bar{q}}. \tag{18}$$

They do not contain radiational heating, and no condensation or evaporation of liquid water are assumed in the subcloud layer; although the equations remain valid if q is total water up into the cloud layer, provided liquid water is carried with the air. There are no equations corresponding to Eqs. (13a) or (9). Indeed, for the constant transition layer case we shall show that

$$\Delta q>\Gamma_q\Delta p.$$

Three new variables have been introduced (F_{0q} is supposed known), and these can be solved for from an initial condition. Further, we can find the cloud base change from a relation

$$\frac{dP}{dt}=A\frac{d\bar{\bar{s}}}{dt}+B\frac{d\bar{\bar{q}}}{dt}, \tag{19}$$

where A and B are known but slowly varying parameters (see Eq. 34).

This paper will explore observationally the validity and consistency of the cloud-subcloud interaction equations [(6), (11), (16) and (17)] as well as compare with observations the solutions of Eqs. (6), (11), (3), (13a), (9), (16), (17), (18), and (19) (for a "steady state" transition layer) *given* α and β.

Table 1 summarizes the model parameters derived from the profiles in Figs. 1, 2 and 3, giving some idea of the variability. We shall use the 1000 and 1400 soundings of Fig. 2 for the budget study. Γ_s and Γ_{Lq} are values for the layer $1.0<\hat{p}<1.2$ just above cloud base.

TABLE 1. Model profile parameters for mean soundings in Figs. 1–3.

Parameter	Units	Fig. 1	Fig. 2 1000 LST	Fig. 2 1400 LST	Fig. 3 Transition layer	Fig. 3 Into cloud
P	mb	125.3	92.4	160.3	84.0	84.3
Δp	mb	13.0	8.5	19.8	9.5	3.9
α		0.10	0.09	0.12	0.11	0.05
Δs	10^3 J kg^{-1}	0.56	0.39	0.65	0.58	0.10
Γ_s	10 J kg^{-1} mb^{-1}	4.3	4.3	3.3	6.1	2.6
$L\Delta q$	10^3 J kg^{-1}	−3.30	−2.48	−3.67	−2.00	(−1.33)*
Γ_{Lq}	10 J kg^{-1} mb^{-1}	−12.1	−12.3	−10.1	−18.5	−14.9

* Due to poor hygristor response above 95% relative humidity.

f. Solution of the non-dimensional equations for constant Δs, $L\Delta q$

Mean profiles (pressure scaled by P) have been presented in Section 3. Since we can determine F_{0s} and F_{0q} from the budget study in Section 5, it is convenient to also non-dimensionalize the equations using free convection velocity and static energy scales (Ω_*/g and S_*, respectively, for the subcloud layer, Deardorff, 1970b). We define

$$\frac{\Omega_*}{g}=\left(\frac{\bar{\rho}F_{0s}P}{\bar{s}}\right)^{\frac{1}{3}}, \tag{20}$$

$$S_*=\left(\frac{F_{0s}^2\bar{s}}{\bar{\rho}P}\right)^{\frac{1}{3}}, \tag{21}$$

where $\bar{\rho}$, $\bar{s}$ are mean values for the subcloud layer. A corresponding q scale is

$$Q_*=gLF_{0q}/\Omega_*. \tag{22}$$

and dimensionless time scale $\tau_*=P/\Omega_*$. Substituting Eq. (9) in (6), (11) and (13a), and denoting non-dimensional values by a caret, the s system reduces to three equations for constant $\Delta\hat{s}$ (dropping the area average symbol)

$$d\hat{\bar{s}}/d\hat{t}=1+(d\hat{P}/d\hat{t}+\hat{\omega}+\hat{\omega}_B^*)\alpha\hat{\Gamma}_s+\hat{\bar{R}}, \tag{23}$$

$$d\hat{\bar{s}}/d\hat{t}=(d\hat{P}/d\hat{t}+\hat{\omega}+\hat{\omega}_B^*-\Delta\hat{\omega}_B^*)\hat{\Gamma}_s+\hat{R}_B, \tag{24}$$

$$\beta=(d\hat{P}/d\hat{t}+\hat{\omega}+\hat{\omega}_B^*)\alpha\hat{\Gamma}_s, \tag{25}$$

with solutions

$$d\hat{\bar{s}}/d\hat{t}=1+\beta+\hat{\bar{R}}, \tag{26}$$

$$\Delta\hat{\omega}_B^*=(\beta-\alpha-\alpha\beta)/\alpha\hat{\Gamma}_s+\Delta\hat{R}/\hat{\Gamma}_s, \tag{27}$$

$$\hat{\omega}_B^*=(\beta/\alpha\hat{\Gamma}_s)-d\hat{P}/d\hat{t}-\hat{\omega}, \tag{28}$$

where

$$\Delta\hat{R}=\hat{R}_B-\bar{\hat{R}}.$$

These solutions may be useful, although Table 1 shows variability in Δs, because still $d\Delta s/dt \ll d\bar{s}/dt$. A rearrangement of (27) and (28) (neglecting $\Delta\hat{R}$) shows the relation of α to β:

$$\alpha=\frac{\beta(d\hat{P}/dt+\hat{\omega}+\hat{\omega}_B^*-\Delta\hat{\omega}_B)}{(\beta+1)(d\hat{P}/dt+\hat{\omega}+\hat{\omega}_B^*)}. \tag{29}$$

In the no-cloud case, where $\omega_B^*=\Delta\omega_B^*=0$, this reduces to $\alpha=\beta/(\beta+1)$ (Betts, 1973; Tennekes, 1973). With cumulus clouds, we see $\alpha<\beta/(\beta+1)$; see Table 3. The corresponding dimensionless $\hat{q}$ equations for $\Delta\hat{q}$ constant are

$$d\hat{\bar{q}}/d\hat{t}=1+(d\hat{P}/d\hat{t}+\hat{\omega}+\hat{\omega}_B^*)\Delta\hat{q}, \tag{30}$$

$$d\hat{\bar{q}}/d\hat{t}=(d\hat{P}/d\hat{t}+\hat{\omega}+\hat{\omega}_B^*)\hat{\Gamma}_q-\Delta\hat{\omega}_B^*\Delta\hat{q}/\alpha. \tag{31}$$

The solutions using (25) and (27) are

$$\Delta\hat{q}=\alpha(\beta\hat{\Gamma}_q-\alpha\hat{\Gamma}_s)/(\beta-\alpha+\alpha\Delta\hat{R}). \tag{32}$$

Typically, $\hat{\Gamma}_q$ is negative, $\hat{\Gamma}_s$ is positive, $\beta-\alpha>0$ and $\Delta\hat{R}$ is very small (over land) so that $\Delta\hat{q}$ is negative and

$$|\Delta\hat{q}|>|\hat{\Gamma}_q\alpha|.$$

In the limiting case of no clouds as $\alpha\to\beta/(\beta+1)$, the solution becomes

$$\Delta\hat{q}=\hat{\Gamma}_q-\hat{\Gamma}_s/(1+\beta).$$

This is a very large negative value since both terms are typically negative. For the time change of $\hat{q}$,

$$d\hat{\bar{q}}/d\hat{t}=1+\beta(\beta\hat{\Gamma}_q-\alpha\hat{\Gamma}_s)/\hat{\Gamma}_s(\beta-\alpha+\alpha\Delta\hat{R}). \tag{33}$$

Again the second term is negative and typically over land larger in magnitude than 1, so that the subcloud layer dries out with time.

Solutions 26 and 32 can be substituted in (see Eq. 19)

$$d\hat{P}/d\hat{t}=\hat{A}d\hat{\bar{s}}/d\hat{t}+\hat{B}d\hat{\bar{q}}/d\hat{t} \tag{34}$$

to give the rate of rise of cloud base. For the data of Fig. 2, $\hat{A}=1.1\times10^{-2}$ and $\hat{B}=-0.5\times10^{-2}$, so that both warming and drying produce a rise of cloud base. This value of $d\hat{P}/d\hat{t}$ can be substituted in (28), giving $\hat{\omega}_B^*$, provided $\hat{\omega}$ is known (or neglected, since typically both ω_B^* and dP/dt are quite large over land in the daytime).

The important role of the parameters $\alpha=\Delta p/P$ and $\beta=F_{s-}/F_{0s}$ in the solutions is clear. Scaling variables

for the dry free convection layer were defined in terms of two bulk parameters (P, F_{0s}) [Eqs. (20) and (21)]. For the subcloud layer two further and in many ways analogous parameters have been introduced, characteristic of the subcloud-cloud layer interface (ΔP, F_{s-}). These four parameters may be summarized in non-dimensional form as the matrix

$$\begin{pmatrix} 1 & \alpha \\ 1 & \beta \end{pmatrix}.$$

This subsection has outlined the solution of the non-dimensional system of equations for $\Delta\hat{s}$, $\Delta\hat{q}$ constant. Numerical values will be substituted in Section 5. These are of particular interest because they indicate the magnitude of the cloud base fluxes, parameters and gradients in terms of the subcloud layer scales Ω_*, S_* and Q_*, as well as the relative magnitudes of α and β.

5. Results

The data which will be used for this analysis were soundings at 1000 and 1400 local time on twenty separate days (in general, not consecutive) of shallow cumulus convection at Carrizal, Venezuela. The twenty 1000 soundings were averaged as in Section 3 by first scaling the pressure by $P=p_0-p_B$ (p_B is the mean lifting condensation level for the subcloud layer) to give a mean 1000 sounding. The twenty 1400 soundings were processed similarly (see Fig. 2). These two mean soundings were used for a single time-step budget calculation, and to test the equations and solutions of Section 4, as well as to derive estimates of α and β. This involves some assumptions.

First, Eq. (1) and the similar equations for $\tilde{q}$ and $\tilde{h}$ and those derived from them were used. This means that horizontal advection of $\tilde{s}$, $\tilde{q}$ and $\tilde{h}$ was neglected in the budget study. This is probably not unreasonable since near local noon the local change terms $\partial\tilde{s}/\partial t$ and $\partial\tilde{q}/\partial t$ are large over land, while horizontal gradients in the tropics are typically small. There is also the likelihood that in the 20-day mean, the mean horizontal advection terms will at least in part cancel, while the local change terms do not, having the same characteristics every day. A second assumption is that $\tilde{\omega}$ will be neglected. The validity of this assumption is less obvious, since the predominant vertical motion field is likely to be subsidence on all the days. However, in the subcloud layer over land, dP/dt is large (18 mb h^{-1} or 5 cm s^{-1}), whereas typical subsidence velocities in suppressed conditions in the tropics are much smaller (2 mb h^{-1}; Holland and Rasmussen, 1973). ω_B^* and $\Delta\omega_B^*$ are themselves both larger than dP/dt near cloud base (but their difference (Eq. 11) is comparable to dP/dt) so the neglect of $\tilde{\omega}$ is probably quite good for this analysis. Both these assumptions are necessary since single station data is being used, but both are probably quite well satisfied because the local time changes dominate. We shall use these average soundings as representative of horizontally averaged fields denoted ($\bar{x}$). We present primarily static energy (s) and latent energy (Lq) fluxes and parameters; virtual static energy fluxes can readily be derived from them.

a. Budget analysis and derived fluxes

The method was to use equations of the form of (2) or (6), but integrated to a variable scaled $\hat{p}=(p_0-p)/P$. The dimensional moist static energy equation was used first. Neglecting $\tilde{\omega}$, and the small change in p_0,

$$P\hat{p}\frac{d\bar{\bar{h}}_p}{dt}=F_{0h}+\hat{p}\frac{dP}{dt}(\tilde{h}_p-\bar{\bar{h}}_p)-F_{ph}+P\hat{p}\bar{R}_p, \quad (35)$$

where $\bar{\bar{h}}_p$, $\bar{R}_p$ denote vertical averages to the level $\hat{p}$, and $\tilde{h}_p$, F_p and ω_p [in Eq. (36)] denote values at that level. The convective flux F_{ph} is parameterized as in (4) in the form

$$F_{ph}=\omega_{ph}^*(h_c-\tilde{h})_p, \quad (36)$$

where a constant value for the cloud h_c equal to the subcloud layer mean ($\bar{\bar{h}}$) was used above cloud base. Betts (1975) showed that the incorporation of entrainment into clouds to change h_{pc} seemed to have little effect on the model. Since ω_p^* will only be computed for a short distance above cloud base, entrainment will be omitted for simplicity. For $\hat{p}=1$ (cloud base), Eq. (35) is the sum of (6) and (16). For the extension of the ω^* model into the subcloud layer (discussed in more detail in Section 5e), we set $h_{pc}=\bar{\bar{h}}_p$.

Net surface radiation (N) was measured during the experiment using a Funk net radiometer, and the thermal flux G into the ground was measured using a vertical array of thermocouples sunk into the ground. Both measurements were made in a standard meteorological enclosure at the observation site, in grassy terrain, roughly representative of the surrounding area. Since measurements were not available for every day, representative mean values for $\langle N\rangle$ and $\langle G\rangle$ for sunny days with scattered small cumulus were derived (Dugan, 1973). The budget computation (35) was initialized by setting

$$F_{0h}/g=\langle N\rangle-\langle G\rangle=524\pm26 \text{ W m}^{-2}. \quad (37)$$

It is difficult to put an accuracy on either of these point measurements. The ground storage was 19% of the incoming net radiation. The total error estimate on $\langle N\rangle-\langle G\rangle$ of $\pm5\%$ is based on a possible systematic bias for the net radiometer. The sensitivity of the results to this probable error is discussed below.

The net radiative source term R for the mean soundings was calculated using longwave (Cox, 1973) and shortwave absorption (Manabe and Strickler, 1964) programs, assuming no clouds. The presence of small cumulus or some cirrus will modify R, but the change is difficult to compute without more detailed

cloud observations. Fortunately, $\bar{R}$ is small near local noon (~ -1 K day^{-1}) as compared with $d\bar{s}/dt$ ($\equiv 1$ K h^{-1}), so the estimates of R using a clear sky are probably acceptable.

Eq. (35) was solved for the convective h flux from the surface to $\hat{p}=1.5$. Fig. 4 shows F_{ph} as a heavy solid line. Equation 36 was then solved for the convective mass flux ω_p^* for $0.9<\hat{p}<1.5$ (light solid line in Fig. 4). In the computation and figures, we have used energy fluxes as F/g (units W m^{-2}), and mass fluxes ω^*/g (units kg m^{-2} s^{-1}). The liquid water static energy flux F_{sl} was then computed as a function of $\hat{p}$ from

$$F_{psl}=\omega_{ph}^*(s_{lc}-\bar{s})_p, \tag{38}$$

where a constant subcloud layer mean value ($\bar{s}$) was used for s_{lc} as in (4) above cloud base, and $\bar{s}_p$ below. The static energy analogue of (35),

$$P\hat{p}\frac{d\bar{s}_p}{dt}=F_{0s}+\hat{p}\frac{dP}{dt}(\bar{s}_p-\bar{\bar{s}}_p)-F_{psl}+P\hat{p}\bar{R}_p, \tag{39}$$

was then solved for F_{0s}, the surface s flux. Finally, the surface moisture flux and Bowen ratio B were computed from

$$LF_{0q}=F_{0h}-F_{0s}, \tag{40}$$

$$B=F_{0s}/LF_{0q}. \tag{41}$$

The validity of the analysis was checked by examining the constancy of B (and hence of the separate F_{0s}, F_{0q} fluxes) as $\hat{p}$ increased from 0.95 to 1.3 (Fig. 5). Since B remained sensibly constant over this range, a mean value was calculated giving

$$F_{0s}/g=252\mp 7 \text{ W m}^{-2},$$
$$LF_{0q}/g=272\pm 33 \text{ W m}^{-2},$$
$$B=0.93\mp 0.14.$$

The error estimates are based on a $\pm 5\%$ change in F_{0h} which changes F_{0s} by $\mp 3\%$ and LF_{0q} by $\pm 12\%$ and B correspondingly, but all remain sensibly constant as in Fig. 5 for $0.95<\hat{p}<1.30$. Using (39), F_{psl} was recomputed with $F_{0s}/g=252$ W m^{-2} and the total water flux (vapor plus liquid) was found from

$$LF_{pqt}=F_{ph}-F_{psl}. \tag{42}$$

These fluxes are also shown in Fig. 4. The F_{sl} flux (F_s below cloud base) shows a negative slope for the entire layer $0<\hat{p}<1.4$ corresponding to warming by the convection (Betts, 1975). There is some indication of slight cooling above $\hat{p}=1.4$. The LF_{qt} flux shows drying by the convection through most of the subcloud layer $0<\hat{p}<0.9$, moistening $0.9<\hat{p}<1.3$ and a larger moistening for $\hat{p}>1.3$. The change in slope of the q and s profiles at the top of the "near well-mixed" layer ($p=0.9$) also appears as a change in the gradient of the corresponding fluxes. The F_h flux shows the very small change of h in the subcloud layer below $\hat{p}=0.85$ and the convective input of h above. Since these flux curves are integrated from the surface, an error in the surface flux just shifts the entire curve, but does not affect the gradients.

If the F_h, LF_{qt} curves (which end at $\hat{p}=1.5$ because of data limitations) are extrapolated, they suggest the convective fluxes become zero below $\hat{p}=2.0$ corresponding to a layer of shallow cumulus.

The dashed profile of ω_{ps}^* in Fig. 4 was recomputed from (38) (replacing ω_h^* by ω_s^*) using the F_{sl} flux (Fig. 4)

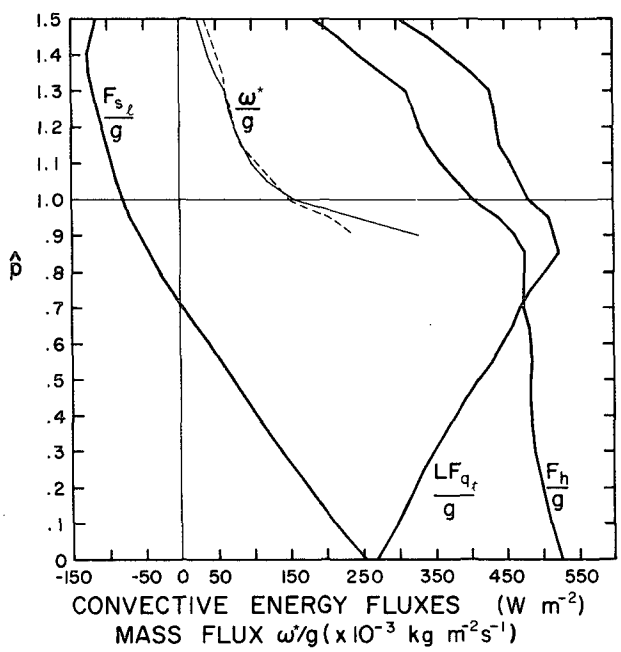

FIG. 4. Energy flux profiles of moist static energy, total water and liquid water static energy for a four-hour period centered on local noon over land in Venezuela (heavy lines). Also shown are the convective mass flux profiles (ω_h^*/g, light solid; ω_s^*/g, light dashed) derived from a simple cloud model. $\hat{p}=1$ corresponds to cloud base.

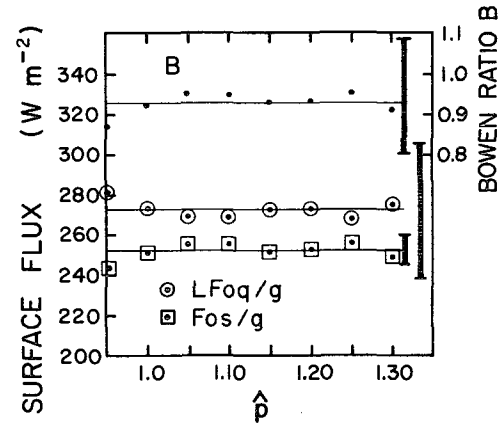

FIG. 5. Surface flux and Bowen ratio estimates derived by integrating the budget equations to a variable height $\hat{p}$. The horizontal lines are the mean values used, and the heavy vertical bars an estimate of the possible systematic error resulting from a $\pm 5\%$ error in F_{0h}, which bodily shifts each family of points.

calculated from (39) with a constant surface flux of $F_{0s}/g=252$ W m^{-2}. The two profiles of ω^* (ω^*_h, ω^*_s) in Fig. 4 agree closely near cloud base (corresponding to the constancy of B in Fig. 5) but less well below cloud base where the parcel-environment differences become small (see Section 5e).

The constancy of B in Fig. 5 and agreement of ω^* in Fig. 4 (as in Betts, 1975) both lend support to the validity of the ω^* model for the convective transports used in Eqs. 6, 16, 36 and 38. The addition of entrainment into clouds does not affect this agreement, although ω^* decreases a little less rapidly with height (as in Betts, 1975).

b. Local change at cloud base

A different although related check on the model which is independent of the actual convective fluxes but depends only on the local flux gradients can be made. This uses the simultaneous pair of cloud base equations (8) and (17), which generalize to (neglecting $\tilde{\omega}$)

$$\frac{\partial F_s}{\partial p}=\frac{d\tilde{s}}{dt}-\hat{p}\frac{dP}{dt}\Gamma_s-R=\omega^*\Gamma_s-\frac{\partial\omega^*}{\partial p}(s_{lc}-\tilde{s})_p, \quad (8')$$

$$\frac{\partial F_q}{\partial p}=\frac{d\tilde{q}}{dt}-\hat{p}\frac{dP}{dt}\Gamma_q=\omega^*\Gamma_q-\frac{\partial\omega^*}{\partial p}(q_{tc}-\tilde{q})_p. \quad (17')$$

Solving this pair of equations simultaneously for ω_* and $\partial\omega_*/\partial p$ using gradients for a shallow layer is a little unstable, particularly below cloud base, where Γ_s and $(s_{lc}-\tilde{s})_p$ become small. Eqs. (8′) and (17′) were solved for the finite difference step from $\hat{p}=1.0$ to 1.1 using the mean soundings and R, giving values corresponding to the level $\hat{p}=1.05$ of

$$\left.\begin{aligned}\omega^*(1.05)/g&=1.5\pm0.5\times10^{-2}\text{ kg m}^2\text{ s}^{-1}\\ &\qquad(1.25\pm0.16\times10^{-2})\\ \frac{\partial\omega^*}{\partial p}(1.05)&=5.1\pm1.7\times10^{-4}\text{ s}^{-1}\quad(4.3\pm0.6\times10^{-4})\end{aligned}\right\}.$$

Numbers in parentheses are the corresponding values at $\hat{p}=1.05$ from Fig. 4, using an average of the two ω^* curves. The agreement is reasonable: the probable error in ω^* found from (8′) and (17′) is large and difficult to estimate: the 33% error assigned is a rough estimate. If the "Bowen ratio" computed as in Section 5a (Eq. 41 and Fig. 5) were found *exactly* constant, then these two methods of calculation of ω_* would give identical results. As it is, the fluctuation in B in Fig. 5, or the difference of the two values of ω_* in Fig. 4, become magnified by inverting (8′) and (17′) for a shallow layer. The analysis in Section 5*a* is a more stable method of finding an ω^* profile with height.

TABLE 2. Scaling parameters.

Parameter	Value	Units
P/g	1288	kg m^{-2}
F_{0s}/g	252	W m^{-2}
LF_{0q}/g	272	W m^{-2}
$\bar{\rho}$	1.09	kg m^{-3}
$\bar{s}$	305.8	10^3 J kg^{-1}
Ω_*/g	2.25	kg m^{-2} s^{-1}
S_*	0.112	10^3 J kg^{-1}
Q_*	0.121	10^3 J kg^{-1}
τ_*	573	s

c. Model parameters from budget analysis

Table 2 gives the subcloud layer scaling parameters, based on the mean surface fluxes and the mean depth of subcloud layer for the 4h period. MKS units used are so as to give the convective "velocity" scale Ω_*/g as a mass flux (kg m^2 s^{-1}), and the static energy and water vapor scaling parameters both in the common units of J kg^{-1}. (The numbers in the table change only slightly if the more familiar units of m s^{-1} and K are used for the velocity and temperature scales.)

Table 3 gives the model parameters for the subcloud layer derived from the data in Figs. 2, 4 and 5 in both dimensional and nondimensional form. The first six variables are given for the two times, together with an average, since none of these variables are the same at the beginning and end of the period. The mean values in parentheses were obtained by averaging the two corresponding dimensionless values: they differ slightly from the simple average of the two dimensional parameters.

The error analysis is quite rough. The main errors, which have been used to estimate errors in the derived parameters, are the probable error in the sample mean cloud base of ±3 mb (see Appendix A) and that in the surface fluxes (see Section 5a). The values in brackets for Γ_s, Γ_{Lq} are subjective. Errors in the radiation flux are uncertain.

Table 3 summarizes several important features of the data set. $\alpha=\Delta p/P=0.11\pm0.02$, that is, the "model" transition layer derived from $\Delta p=\Delta s/\Gamma_s$ is only 11% of the depth of the subcloud layer in the mean. The closure parameter β defined as a ratio of fluxes by (13a) is $\beta=0.41\pm0.05$. This is considerably more than previous estimates for dry convection. However, β_v, defined as the ratio of the *virtual* static energy fluxes, is smaller:

$$\beta_v=(dP/dt+\omega^*_B)\Delta s_v/F_{0s_v}=0.21\pm0.03.$$

This value is comparable to previous estimates (Tennekes, 1973; Deardorff, 1974a). A corresponding α_v is also smaller

$$\alpha_v=\Delta s_v/\Gamma_{s_v}P=0.08\pm0.02.$$

We note that in agreement with (29), α is significantly less than $\beta/(\beta+1)$ in sharp contrast with the dry mixed layer model (Betts, 1973). This can be attributed to the

TABLE 3. Model parameters derived from the data.*

Dimensional parameter	Units	Value at 1000 LST	Value at 1400 LST	Mean value	Dimensionless value	Value at 1000 LST	Value at 1400 LST	Parameter
P	mb	92.4	160.3	126.4±3	1			
Δp	mb	8.5	19.8	(13.8)±3	0.11±0.02	0.092	0.123	α
Δs	10^3 J kg^{-1}	0.37	0.65	0.51±0.08	4.5±0.7	3.3	5.8	$\Delta\hat{s}$
$L\Delta q$	10^3 J kg^{-1}	−2.48	−3.67	−3.1±0.4	−25.4±3	−20.5	−30.3	$\Delta\hat{q}$
Γ_s	10 J kg^{-1} mb^{-1}	4.3	3.3	(3.7)(±0.3)	41.2(±4.5)	35.6	47.0	$\hat{\Gamma}_s$
Γ_{Lq}	10 J kg^{-1} mb^{-1}	−12.3	−10.1	(−10.9)(±0.5)	−114.0(±6)	−94.2	−133.8	$\hat{\Gamma}_q$
F_{0s}/g	W m^{-2}			252∓7	1			$\hat{F}_{0s}$
LF_{0q}/g	W m^{-2}			272±33	1			$\hat{F}_{0q}$
F_{Bs}/g	W m^{-2}			−79∓8	−0.31±0.05			$\hat{F}_{Bs}$
$\frac{1}{g}\left(F_{Bs}+\frac{dP}{dt}\Delta s\right)$	W m^{-2}			−103∓9	−0.41±0.05			$-\beta$
$\bar{R}$	W m^{-2}			−17	−0.07			$\hat{\bar{R}}$
ΔR	W m^{-2}			2	0.01			$\Delta\hat{R}$
LF_{Bq}/g	W m^{-2}			483±35	1.78±0.08			$\hat{F}_{Bq}$
$\frac{1}{g}\left(F_{Bq}+\frac{dP}{dt}\Delta q\right)$	W m^{-2}			630±35	2.30±0.12			
$\frac{1}{g}\frac{dP}{dt}$	10^{-3} kg m^{-2} s^{-1}			48±3	2.1 10^{-2} ±0.1			$\frac{d\hat{P}}{dt}$
ω_B^*/g	10^{-3} kg m^{-2} s^{-1}			156±20	6.9 10^{-2}±0.9			$\hat{\omega}_B^*$
$\Delta\omega_B^*/g$	10^{-3} kg m^{-2} s^{-1}			110±14	4.9 10^{-2}±0.6			$\Delta\hat{\omega}_B^*$
$\partial\omega_B^*/\partial p$	10^{-4} s^{-1}			7.9±1.0	4.4 10^{-1}±0.6			$\partial\hat{\omega}_B^*/\partial\hat{p}$

* Mean values in parentheses were obtained by averaging the two dimensionless values. Errors in parentheses are subjective.

appreciable size of $\Delta\omega_B^*$. Eq. (29) predicts the relation between both pairs (α,β) and (α_v,β_v) quite well, even though Δs (and Δs_v) both increase during the four hour period, because

$$\frac{d\Delta s}{dt} \ll \frac{d\bar{\bar{s}}}{dt}.$$

$\Delta\omega_B^*=(\partial\omega_B^*/\partial p)\,\Delta p$ is comparable in size to ω_B^*, so it is certainly not negligible in (11) or (29) [$\partial\omega_B^*/\partial p$ was estimated as the gradient in the layer $0.95<\hat{p}<1.05$]. Physically, this means the heating due to the net convection at cloud base, which is

$$(\omega_B^*-\Delta\omega_B^*)\Gamma_s,$$

is much less than $\omega_B^*\Gamma_s$, although the cloud base fluxes are still proportional to ω_B^*. Indeed, the cooling due to detrainment is 70% of the heating due to compensating subsidence between clouds (see also Betts, 1975). The determination of $\Delta\omega_B^*$ from the data is however subject to an appreciable margin of error because $\partial\omega_B^*/\partial p$ changes rapidly near cloud base. We have chosen to evaluate $\partial\omega_B^*/\partial p$ centered an $\hat{p}=1.0$ for consistency with Δs [Eqs. (9) and (11)] and ω_B^* which are also evaluated at $\hat{p}=1.0$ (cloud base). It could be argued that this is inconsistent with the determination of Γ_s for which the layer just above cloud base $(1.0<\hat{p}<1.2)$ was used so as to give a more stable estimate. However, the conclusions of the paper are unchanged if Γ_s is also estimated for the layer $0.95<\hat{p}<1.05$.

Note that the ratio of the cloud base flux $\omega_B^*\Delta s$ to F_{0s} is -0.31 ± 0.05. This is rather less in magnitude than β, which includes the additional cloud base term of $\Delta s\, dP/dt$, which can be regarded as a consequence of the averaging to form the mixed layer, for which $\bar{\bar{s}}<s_B$. The cloud base flux is a small but significant contribution to the warming of the subcloud layer. In contrast, the cloud base latent energy flux is greater than the surface latent energy flux in agreement with the strong drying observed. We note that the ratio of $LF_{Bq}/F_{Bs}=L\Delta q/\Delta s$ is imposed by the model, so that to explain the large cloud base latent energy flux we must explain $L\Delta q$. The steady state transition layer model (Sections 4f and 5d) provides a partial explanation in terms of α, β and gradients in the cumulus layer.

The magnitudes of the dimensionless parameters in Table 3 are themselves of interest. $\Delta\hat{s}$ and $\hat{\Gamma}_s$ are large, reflecting the fact that the cumulus layer represents a strong stable layer to the subcloud layer *dry* turbulence (but not of course to that fraction which reaches its condensation level). $\Delta\hat{q}$ and $\hat{\Gamma}_q$ are correspondingly even larger. α, $\Delta\hat{s}$, $\Delta\hat{q}$, $\hat{\Gamma}_s$, $\hat{\Gamma}_q$ all increase by 25 to 50% of their mean value during the period (although Γ_s, Γ_{Lq} decrease) so that the layer is not really in a steady state. However, Δs in particular (and $\Delta p=\Delta s/\Gamma_s$) is small and very sensitive to small fluctuations in the data as well as small errors in cloud base so that other data is needed to see if these changes are typical. The dimensionless cloud base mass-flux parameters are only 5–7% of Ω_*. This small value of $\hat{\omega}_B^*$ (0.07) suggests that only a small fraction of the subcloud layer turbulence rises through cloud base to form clouds; thus giving some retrospective justification for the separation

of the problem into two distinct layers, cloud and subcloud; and of the use of closure (13a) based on a kinetic energy budget for the subcloud layer turbulence. However, we shall show in Section 5e that the fraction of the subcloud layer mass flux rising to form clouds is more like 25% than 7%.

d. *Comparison with the solutions for constant Δs, $L\Delta q$ for the transition layer*

Table 3 shows that the assumption of Δs, $L\Delta q$ constant is not too good for this data set. However, $d\Delta s/dt < d\bar{s}/dt$, although the corresponding inequality for $L\Delta q$ is not so well satisfied. It is, therefore, of interest to compare parameters derived from the budget with those obtained by inserting mean parameters from Table 3 into the solutions for constant Δs, $L\Delta q$ derived in Section 4 (Eqs. 26, 27, 28, 32, 33 and 34). Table 4 presents the comparison. The bracketed values represent no comparison, since β was derived from the s budget and the "observed" $(\hat{\omega}_B^* + d\hat{P}/d\hat{t})$ is exactly $\beta/\alpha\hat{\Gamma}_s$. This means that the model value of $\hat{\omega}_B^*$ can differ from the observed value only through a difference in $d\hat{P}/d\hat{t}$. The only true independent tests of the steady state transition layer model are the predictions of $\Delta\hat{\omega}_B^*$, which compares quite well with that observed, and the water vapor parameters $\Delta\hat{q}$ and $d\hat{q}/dt$ which compare rather less well. The steady-state solution underestimates $\Delta\hat{q}$ by 25%, which results in a still larger underestimate of $d\hat{q}/d\hat{t}$, the rate at which the subcloud layer dries out. The underestimate of $d\hat{q}/d\hat{t}$ leads to a slight underestimate of $d\hat{P}/d\hat{t}$, the rate of rise of cloud base (which is dominated by $d\hat{s}/d\hat{t}$).

Eq. (29), which relates α to β and the cloud base flux parameter, is satisfied exactly using the model steady state solutions. The value $\alpha = 0.13$ is given by substituting *observed* values for $\Delta\hat{\omega}_B^*$ instead of the model prediction in (29).

Eq. (49) between α, β and γ, which is satisfied for Δs, $L\Delta\hat{q}$ constant, is discussed in Appendix B.

We conclude that if α, $\Delta\hat{s}$ and $\Delta\hat{q}$ change considerably in the time period of interest, as they appear to do in this data centered on local noon over land, then the steady state model will give only qualitatively satisfactory results for the water vapor budget. The water vapor budget is poor because $d\hat{q}/d\hat{t}$ results from the *difference* between the surface flux and the cloud base flux which is large and sensitive to errors in the predicted value of $\Delta\hat{q}$. Eq. 29 relating α, β and the cloud base fluxes, as well as the detrainment parameter $\Delta\omega_B^*$, are predicted somewhat better ($\pm 15\%$), but clearly further tests of the usefulness of the steady state model are needed.

e. *Structure of the subcloud layer and unresolved questions*

The model presented in Section 4 treats the subcloud layer as well mixed. The profiles shown in Figs. 1–3 show the extent to which this is an approximation: the static energy has a minimum near $\hat{p} = 0.4$, while the specific humidity (Lq) falls with height. The weak stable stratification of s and steeper gradient of Lq in the

TABLE 4. Comparison of steady state model and observed parameters.*

Parameter	Equation	Steady-state model		Observed
$\frac{d\hat{P}}{d\hat{t}}$	(34)	$\hat{A}\frac{ds}{d\hat{t}} + \hat{B}\frac{d\hat{q}}{d\hat{t}}$	1.8×10^{-2}	$2.1\pm0.1\times10^{-2}$
$\hat{\omega}_B^* + \frac{d\hat{P}}{d\hat{t}}$	(28)	$\beta/\alpha\hat{\Gamma}_s$	9.0×10^{-2}	$(9.0\pm0.9\times10^{-2})$
$\hat{\omega}^*$	(28)	$\beta/\alpha\hat{\Gamma}_s - \frac{d\hat{P}}{d\hat{t}}$	7.2×10^{-2}	$6.9\pm0.9\times10^{-2}$
$\Delta\hat{\omega}_B^*$	(27)	$\frac{\beta-\alpha-\alpha\beta}{\alpha\hat{\Gamma}_s} + \frac{\Delta\hat{R}}{\hat{\Gamma}_s}$	5.7×10^{-2}	$4.9\pm0.6\times10^{-2}$
$\frac{d\hat{s}}{d\hat{t}}$	(26)	$1+\beta+\hat{R}$	1.34	$(1.34\pm.05)$
Δq	(32)	$\frac{\alpha(\beta\hat{\Gamma}_q - \alpha\hat{\Gamma}_s)}{\beta-\alpha+\alpha\Delta\hat{R}}$	-18.7	-25.4 ± 3
$\frac{d\hat{q}}{d\hat{t}}$	(33)	$1+\frac{\beta(\beta\hat{\Gamma}_q - \alpha\hat{\Gamma}_s)}{\hat{\Gamma}_s(\beta-\alpha+\alpha\Delta\hat{R})}$	-0.70	-1.32
α	(29)	$\frac{\beta(d\hat{P}/d\hat{t}+\hat{\omega}_B^*-\Delta\hat{\omega}_B^*)}{\beta+1(d\hat{P}/d\hat{t}+\hat{\omega}_B^*)}$	0.11 model fluxes 0.13 observed fluxes	(0.11) 0.11 ± 0.02
γ	(49)	$\beta-\alpha-\alpha\beta$	0.25	0.22 ± 0.05

* Values in parentheses were used to derive α and β.

upper part of the subcloud layer are consistent with the small downward heat flux and large upward moisture flux at cloud base (Fig. 4). Mahrt (1976) has also noted this. It is of interest to see whether the subcloud layer profiles are similar if suitably scaled. Scaled using the surface flux parameters S_*, Q_*, they are not. Table 3 shows, for example, that $\Delta\hat{q} \gg \Delta\hat{s}$. However, scaled by the cloud base jumps Δs, $L\Delta q$ (which are proportional to the cloud base fluxes), the s and Lq profiles in the upper part of the subcloud layer become more nearly similar. Fig. 6 (heavy curves) shows the profiles of $(\bar{s}_p-\bar{\bar{s}})/\Delta s$ and $(L\bar{q}_p-L\bar{\bar{q}})/L\Delta q$ averaged for the 1000 and 1400 mean soundings. Both functions are unity at $\hat{p}=1$ (cloud base) but while the profiles show some agreement near cloud base, they diverge below. Fig. 6 (light curves) shows the profiles scaled by the mean differences from cloud base $\hat{p}=1.0$ to $\hat{p}=0.4$ where $\bar{s}$ has a minimum. In this case, agreement of the curves is forced at $\hat{p}=0.4$ and 1.0. Agreement between the s and Lq profiles is now very close. Thus, it seems likely that the profiles of s and Lq are in some sense similar in the upper part of the subcloud layer, but the appropriate scaling parameters are not clear.

A related question is whether $\bar{\bar{s}}$, $L\bar{\bar{q}}$ are good estimates of cloud base properties (assumed in Eq. 5), in view of the subcloud gradients of s and Lq. This assumption couples the cloud base fluxes in the ratio $\Delta s/L\Delta q$. Dry convective elements originate presumably from the surface superadiabatic layer, but since the exact source region and degree of subsequent turbulent mixing in the subcloud layer are unknown, it is hard to estimate cloud base properties.

Another question of interest is whether the mass flux model (Eq. 5) can be extended into the subcloud layer. This also depends on the specification of mean properties for a model convective parcel in this layer. A simple *diagnostic* solution will be given here, based on the derived convective fluxes in Fig. 4. It is clearly inappropriate to assume that convective parcels have mixed layer properties $\bar{\bar{s}}$, etc. (averaged up to cloud base) at all heights. Instead, we shall assume that the model convective parcel properties at a given height are the average properties *below* that height, i.e.,

$$s_{pc}=\frac{1}{(p-p_0)}\int_{p_0}^{p}\bar{s}dp=\bar{\bar{s}}_p, \qquad (43)$$

where the suffix pc now denotes convective element at a pressure level p. In terms of an entraining parcel model, this has the specific meaning that the entrainment rate (λ) is inversely proportional to the pressure height above the surface

$$\lambda=1/(p_0-p)\ \text{mb}^{-1},$$

which is not unreasonable. (However, Eq. 5 for the cloud base flux requires that at cloud base $s_{pc}=\bar{\bar{s}}$ exactly.) This gives a reasonable profile of parcel

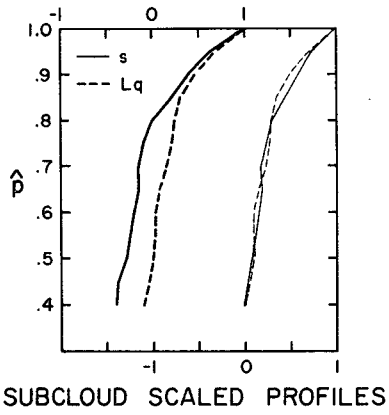

FIG. 6. Scaled subcloud profiles of s and Lq: heavy profiles (upper scale) are scaled by cloud-base jumps Δs, $L\Delta q$, light profiles (lower scale) by the mean differences from $\hat{p}=0.4$ (where $\bar{s}$ has a minimum) to $\hat{p}=1.0$ (cloud base).

properties with height. In particular, the parcel is warmer than the mean for $0.1<\hat{p}<0.7$ and cooler above (see Fig. 7) corresponding to the change of sign of F_s in Fig. 4. Convective mass fluxes were computed using these parcel properties from expressions of the form

$$F_s=\omega_s^*(s_{pc}-\bar{s}_p)$$

from F_s and F_h, for $\hat{p}$ levels from 0.1 to 1.0 (cloud base). These values of ω_h^*, ω_s^* are plotted in Fig. 7 together with a few values above cloud base from Fig. 4. Values of ω_s^* are off-scale and omitted from $\hat{p}=0.55$ to 0.75 where $(s_c-\bar{s})\approx 0$. Although the points show much more scatter in the subcloud layer where the parcel-mean differences are small, there is general agreement on the magnitude of the convective mass flux associated with the fluxes of s and h. In particular, there is general agreement between ω_s^* and ω_h^* estimated independently from F_s and F_h (except where $s_c-\bar{s}\approx 0$). The dashed line is drawn by eye. The profile data are probably unreliable below $\hat{p}=0.15$, as mentioned earlier because the surface data are suspect.

The subcloud layer convective mass flux has a magnitude of approximately 0.6 kg m^{-2} s^{-1} at $\hat{p}\approx 0.3$, which is 0.27 Ω_*/g. Willis and Deardorff (1974) in a laboratory model of a convectively mixed layer found vertical velocity variance

$$\sigma_w\approx 0.65\ W_*$$

where W_* is a convective velocity scale corresponding to our Ω_*/g. Warner (1972) found $\sigma_w\approx 0.7\ W_*$ at $\hat{p}\approx 0.3$ and Pennell and Lemone (1974) found $\sigma_w\approx 0.6\ W_*$. If the fractional area of ascending convective elements is $A\approx 0.4$ (from Deardorff, 1970a, 1972), then one could roughly estimate the convective mass flux as

$$\frac{A}{1-A}0.65\frac{\Omega_*}{g}\approx 0.43\frac{\Omega_*}{g},$$

which is somewhat larger than the estimate given by

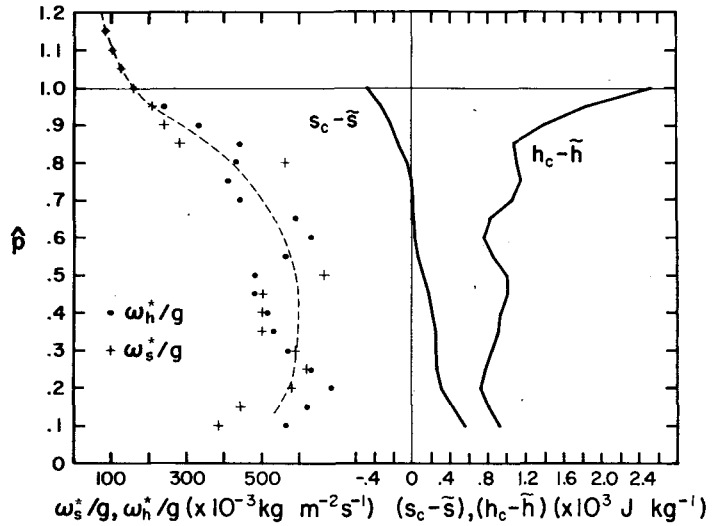

FIG. 7. Convective mass flux estimates in the subcloud layer. ω_h^* (dots) are derived from F_h (Fig. 5) and a parcel environment difference $(h_c-\tilde{h})$ shown: similarly, ω_s^* (crosses) from F_s and $(s_c-\tilde{s})$. $\hat{p}=1$ is cloud base. The dashed line is a profile drawn by eye.

Fig. 7. This is not unreasonable, however, since there will not be a perfect correlation between ascending motion and temperature excess.

Fig. 7 shows the sharp fall of ω^* below cloud base, indicating that only a small fraction of the mass flux ($\sim$25%) reaches cloud base. This is, however, a much larger fraction that $\hat{\omega}_B^*=\omega^*/\Omega_*$. This brings into question the usefulness of Ω_*, S_*, Q_* as scaling parameters above the surface layer. These scales are based on the surface fluxes; but above the surface, the convective fluxes of s and q change in opposite senses. We have already remarked that cloud base fluxes involve different scales (here Δs, $L\Delta q$). Fig. 7 shows that a budget analysis can also provide a consistent subcloud mass-flux, and convective s, Lq, and h perturbations which differ considerably from Ω_*, S_* and Q_*.

This section has explored some of the unresolved questions concerning subcloud layer structure. It appears that the mass flux transport model for convection is useful in the subcloud layer. This model explains quite well the coupling of the static energy and moisture fluxes, and the sharp gradient of convective mass flux across the transition layer at cloud base. Although (43) is an assumption, it also implies that the subcloud mean gradients of s and Lq are coupled. Fig. 6 presents some simple attempts at scaling the static energy and moisture profiles, but clearly this needs further study.

This diagnostic study has not, however, discovered any basic inconsistency in the use of a well mixed subcloud layer model for cumulus parameterization. However, it is still unclear how close cloud base properties are to mixed layer averages.

6. Summary and conclusions

This paper has developed a mixed layer model for the subcloud layer and its interaction with an overlying shallow cumulus layer. The model combines those presented in Betts (1973, 1975). The model involves two important parameters: the ratio $-\beta$ of a model heat flux just below cloud base to the surface heat flux and the ratio α of the depth of a model transition layer just below cloud base to the depth of the subcloud layer. The model transition layer is defined in terms of Δs, the difference between cloud base static energy and that of the mixed layer, and the stratification of $\tilde{s}$ in the cumulus layer. The two parameters α and β relate cloud base mass flux and mass flux gradient to essentially subcloud layer parameters (if the cumulus layer stratification is given). The cloud mass flux model is used to couple the heat and moisture fluxes so that α, β also determine the moisture budget of the subcloud layer (given the surface fluxes) and the rate of change of cloud base height. Predictions are presented for the simple case of a steady state transition layer (Section 5d).

Data from a field experiment over Venezuela are presented showing the mean subcloud layer structure using a scaled pressure coordinate in which cloud base is equivalent to $\hat{p}=1$, and a simple budget study is given for a four hour period centered on local noon based on the model. The subcloud layer structure shows a layer nearly well mixed in s with a minimum at $\hat{p}\approx 0.4$, and a transition layer stabilization starting at $\hat{p}\approx 0.9$. The mean subcloud profiles show a steady decrease of moisture with height, with a steeper gradient above $\hat{p}\sim 0.85$, except for a mean profile generated from

rawinsonde ascents which entered cloud base. During the four hour period used for the budget study, the subcloud layer warms and dries with a corresponding rise of cloud base. The model is used to couple the cloud base fluxes and compute the covective fluxes as a function of pressure from the total surface moist static energy flux, which was found from the measured surface energy budget. Just above cloud base the static energy flux is small and downward (−0.3 times the surface flux) while the latent energy flux is large and upward (1.78 times the corresponding surface flux). The convective flux curves (Fig. 4) show a noticeable change of slope at the top of the nearly well mixed layer ($\hat{p}\approx 0.9$), corresponding to the change of gradient of s and Lq. This is a little below cloud base. The model equations appear to give satisfactory results both for the fluxes and the cloud mass flux as a function of height. However, the model was used to derive them, and no independent test on their validity exists. The derived Bowen ratio of 0.9 is reasonable for the relatively dry terrain.

The fluxes calculated from this budget are used to compute the model parameter β ($=0.41$) while $\alpha=0.11$ is found from the mean structure itself. As predicted by the model, α is considerably less than β for the subcloud layer. The corresponding parameters derived from virtual static energy fluxes and structure are smaller $(\alpha_v,\beta_v)=(0.08, 0.21)$. The data show a large detrainment of cloud mass flux near cloud base that produces a cooling equal to -70% of the convective heating associated with "compensating subsidence."

Model predictions based on the assumption of a steady state transition layer were compared with the budget study results. They showed qualitative agreement. Probably for convection over the sea, a steady state model would be a much better approximation. The time period studied indicated considerable change in the transition layer parameters. These are, however, rather sensitive to small errors in the cloud base estimate, so their time change over land needs further study.

The mass flux model was shown to give a reasonable description of the subcloud layer fluxes (Section 5e). The mass flux in the subcloud layer was found to be only 0.27 of Ω_*, the mass flux analogue of the free convective scale. The problems of determining parcel properties for the dry convection and of scaling the subcloud layer mean profiles were discussed but not resolved. The mixed layer model still seemed a reasonable approximation for the subcloud layer.

In conclusion, the coupling of a mixed layer model to a cumulus mass flux parameterization gives a satisfactory diagnostic tool for the analysis of the time dependence of the subcloud layer and its interaction with an overlying shallow cumulus layer. Further diagnostic and theoretical studies are needed to explore the variability of the parameters α and β used in the model, but it appears that this model could have predictive usefulness.

APPENDIX A

Corrections for Thermal Lag of Thermistor and Hygristor

The radiosonde used in the VIMHEX-1972 experiment was the VIZ 1290 series National Weather Service sonde. This sonde had a new humidity duct designed to reduce the large humidity errors of earlier model sondes (Friedman, 1972). In-field tests (Riehl and Betts, 1972) indicated that the residual errors in humidity were rather small. Nonetheless, thermal lag corrections were made for both the thermistor and hygristor, since both lag errors affect the lifting condensation levels used to estimate cloud base.

Unfortunately, the lag characteristics of the two sensors in current use are not yet well documented. We have used estimates from an unpublished paper (Williams and Acheson, 1976) who analyzed the lag characteristics of these same sensors, which were used in a similar configuration in the GATE experiment. Their recommended equations for the time constants of thermistor (τ_t) and hygristor (τ_h) in seconds are

$$\tau_t=9.8(\rho w)^{-0.43},$$
$$\tau_h=52(\rho w)^{-0.71},$$

where ρ is the air density and w the air speed relative to the sensor. For this subcloud layer study, mean values were used based on a mean radiosonde rise rate of $w=4.8$ m s^{-1}. These were converted to a pressure lag in the vertical

$$\pi_t=-\rho g w\lambda_T=-2.5 \text{ mb},$$
$$\pi_h=-\rho g w\lambda_H=-8.2 \text{ mb}.$$

Since the data were only available at "contact points" every 10 mb and are used here in averages, only a simple correction procedure was used. The true thermistor and hygristor temperatures were taken as

$$T=T_t-\frac{\Delta T_t}{\Delta p}\pi_t,$$
$$T_h=T_t+\frac{\Delta T_t}{\Delta p}(\pi_h-\pi_t),$$

where T_t ($<T$) is the temperature measured by the thermistor, T is the true air temperature, T_h ($>T_t$) the temperature of the hygristor, and $\Delta T_t/\Delta p$ is the lapse of temperature measured by the thermistor for the preceding pressure interval (except for the first sonde level where a forward pressure step was used). Typical corrections in the nearly dry adiabatic subcloud layer are

$$T-T_t\approx -0.2 \text{ K},$$
$$T_h-T_t\approx +0.5 \text{ K}.$$

This hygristor temperature and the measured relative humidity were used to find the specific humidity. The correction to the specific humidity is $\sim+0.5$ g kg^{-1}. The corrections make the subcloud layer slightly cooler and moister, and consequently, lower the cloud base estimate based on lifting condensation level pressure (LCLP) by $\sim$9 mb.

The thermistor correction is rather small and probably sufficiently accurate, but the accuracy of the corrected humidities is less certain. Betts *et al.* (1974) estimated the relative lag between thermistor and hygristor to be only 3 mb (rather than the 5.7 mb given by the above formulas) using a sample of ascents through cloud base. Correspondingly, Fig. 3 shows the timed measurements of cloud base to be slightly above (-2 ± 6 mb) the estimate based on the subcloud layer mean LCLP. Two further effects have been neglected in the humidity correction. Residual solar heating of the hygristor may be present although the sensor is shielded. The hygristor itself has a small time constant in its response to changes in the relative humidity. Both would lead to an underestimate of the true mixing ratio in the subcloud layer. However, the LCL's in Fig. 3 suggest that the corrected humidities may, if anything, be slightly too moist.

We conclude that the corrections for sensor errors are still poorly known, but the systematic errors in the mean profiles presented here are probably <0.1 K for temperature, $\lesssim 0.2$ g kg^{-1} for mixing ratio and $\lesssim 3$ mb for LCLP's.

APPENDIX B

Transition Layer Budget and Closure

Although we have defined a parameter Δp and referred to it as the thickness of a model transition layer, a formal budget equation for this layer is never used. However, for the case of a steady state model transition layer (Δs, Δp constant), Eq. 11 is also the transition layer budget equation. The two convection parameters define the fluxes at the top and bottom of the transition layer ($-\omega_B^*\Delta s$ and $-\Delta\omega_B^*\Delta s$, respectively). This interpretation is important to the closure problem (Section 4c), so it is discussed here using an analysis similar to Betts (1974).

Integrating Eq. (1) through the transition layer thickness Δp gives [analogous to Eq. (6); the "jump" Δs is included in the p integration]

$$\Delta p\frac{d}{dt}\bar{s}_t=\Delta F_s+\frac{dP}{dt}\Delta s+(\bar{\bar{s}}-\bar{s}_t)\frac{d}{dt}\Delta p + \int_P^{P-\Delta p}\tilde{\omega}\frac{\partial\tilde{s}}{\partial p}dp+R_t\Delta p, \quad (44)$$

where the suffix t denotes an average with respect to pressure through the transition layer and ΔF is the convective flux difference. In (44), $\bar{s}_t$ and $\int\tilde{\omega}\partial\tilde{s}/\partial p dp$ depend on the *profile* of s in the transition layer. The simple mixed layer model supposes $\tilde{s}=\bar{\bar{s}}$ below cloud base, with a jump Δs just *below* cloud base P. With this simplification, $\bar{s}_t=\bar{\bar{s}}=\bar{s}_B-\Delta s$, and (44) transforms to

$$\Delta p\frac{d\bar{s}_B}{dt}=\Delta F_s+\left(\frac{dP}{dt}+\tilde{\omega}_B\right)\Delta s+\Delta p\frac{d}{dt}\Delta s+R_t\Delta p. \quad (45)$$

A comparison of terms with (11) shows that

$$\Delta F_s\equiv(\omega_B^*-\Delta\omega_B^*)\Delta s-\Delta p\frac{d\Delta s}{dt}+(R_B-R_t)\Delta p. \quad (46)$$

The difference of the radiative heating rates between the transition layer and cloud base is generally small, and the second term, which vanishes for a steady state transition layer, is usually rather smaller than the first ($\sim$15% for the data in Section 5). Thus, approximately

$$\Delta F_s\approx(\omega_B^*-\Delta\omega_B^*)\Delta s. \quad (47)$$

Using (5) for the cloud base flux it is clear that the static energy flux at the transition layer base has been modeled as $-\Delta\omega_B^*\Delta s$. Fig. 8 shows the model $\tilde{s}$ profile and associated F_{s_l} flux up through cloud base for a steady state transition layer with no vertical gradients of R. The flux gradient is constant through the well-mixed subcloud layer passing through $-\Delta\omega_B^*\Delta s$ at the transition layer base, increasing to a maximum negative of $-(dP/dt+\tilde{\omega}_B+\omega_B^*)\Delta s$ just below the jump of Δs at cloud base, and changing discontinuously to $-\omega_B^*\Delta s$ at cloud base.

Observed atmospheric mean profiles never show the model discontinuity, which is really a construct of the vertical averaging (Deardorff *et al.*, 1974). Indeed Figs. 1 to 3 show a smooth change of $\tilde{s}$ through the transition layer Δp, with a gradient very close to Γ_s above cloud

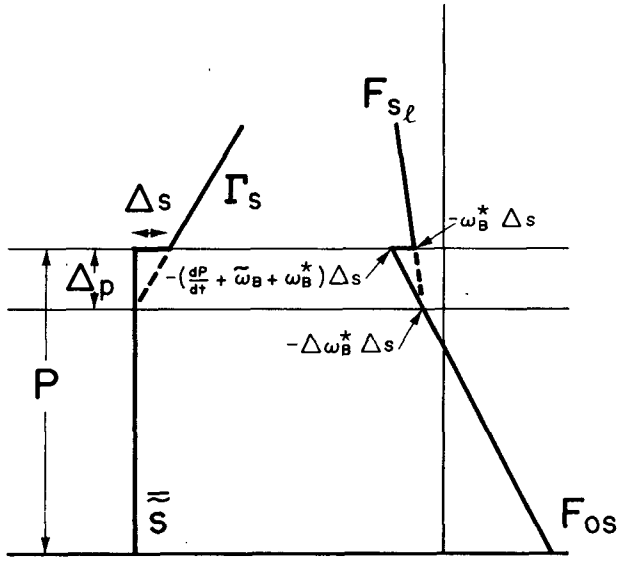

FIG. 8. Model $\tilde{s}$ and F_s, F_{s_l} profiles showing model jumps at cloud base (solid lines) and corresponding profiles (dashed) without the model jumps.

base. To show that the above arguments are essentially unaffected, whatever the profile of $\bar{s}$, Fig. 8 also shows (dashed) the corresponding flux profile for the case where $\partial\bar{s}/\partial p$ is continuous through cloud base into the transition layer. Clearly, this is a closer approximation to observed mean profiles. There is no jump in the flux or change in the flux gradient at cloud base. (Since $\bar{s}$ as defined in Section 4a includes the transition layer, there will be a small adjustment in the s and F_s profiles below the transition layer, which we will not consider.) The full equation corresponding to (45) is

$$\Delta p\frac{d\bar{s}_B}{dt}=\Delta F_s+\left(\frac{dP}{dt}+\tilde{\omega}_t\right)\Delta s+\tfrac{1}{2}\Delta p\frac{d}{dt}\Delta s -\tfrac{1}{2}\Delta s\frac{d}{dt}\Delta p+R_t\Delta p. \quad (48)$$

Eq. (47) is still approximately satisfied: the last terms disappear for constant R, Δp and Δs (indeed the fourth and fifth terms cancel for constant Γ_s) although one further approximation is necessary:

$$\tilde{\omega}_t=\tilde{\omega}_B\left(1-\frac{\Delta p}{2P}\right)\approx\tilde{\omega}_B.$$

The small variation of $\tilde{\omega}$ through the shallow transition layer can be neglected, although that of ω^*, which is large, cannot.

Using data from Fig. 4 and Table 3, we find that (47) is approximately satisfied for the model transition layer Δp $(0.89<\hat{p}<1.0)$:

$$23.7=\Delta F_s/g\approx(\omega^*_B-\Delta\omega^*_B)\Delta s/g=23.5\text{ W m}^{-2}.$$

Such close agreement is fortuitous, since such a shallow layer is involved.

It must be emphasized that $\Delta\omega^*_B$ is not ω^* at the transition layer base, which would diverge to ∞ there as $s_c-\bar{s}\to 0$. $\Delta\omega^*_B$ is a parameter constructed from the cloud base $\partial\omega^*/\partial p$, Δs to represent the flux $(\Delta\omega^*_B\Delta s)$ at the transition layer base. $\Delta\omega^*_B\Delta s$ *can* be interpreted, however, as a convective flux "detrained" in the transition layer, producing a cooling which partly offsets the convective heating $\omega^*_B\Delta s/\Delta p$. In the extreme but unrealistic case of no detrainment, ω^* is constant through the transition layer, $\Delta\omega^*_B=0$, the convective heating rate is $\omega^*_B\Delta s/\Delta p$ and the model reduces to that proposed in Betts (1973). The convective elements "detrained" in the transition layer have not reached their condensation level so they can also be associated with the erosion (cooling) of the transition layer by subcloud turbulence.

Fig. 8 for a mixed layer capped by an inversion just below cloud base does present two clear alternatives for closure, depending on the choice of F_{s-} in (12). These are

$$-\left(\frac{dP}{dt}+\tilde{\omega}_B+\omega^*_B\right)\Delta s=-\beta F_{0s}, \quad (13a)$$

$$-\Delta\omega^*_B\Delta s=-\gamma F_{0s}. \quad (13b)$$

Eq. (13a) could be interpreted using the solid curves in Fig. 8. The "subcloud convection" flux increases to a maximum negative value just below the (model) inversion of $-(dP/dt+\tilde{\omega}_B+\omega^*_B)\Delta s$, where it falls sharply to zero, just as the "cumulus" flux jumps to $-\omega^*_B\Delta s$. A similar interpretation of (13b) and the dashed curves in Fig. 8 as the sum of two processes is that the "subcloud convection" flux reaches a maximum of $-\Delta\omega^*_B\Delta s$ at the base of the transition layer and then decreases linearly to zero (as this component is detrained) while the "cumulus" flux increases linearly from zero to $-\omega^*_B\Delta s$. Although the second model is a little more realistic, only the first simplifies to the dry mixed layer as the cumulus component goes to zero (14), and for this reason (13a) was used to close the equation set. Fortunately, it can be shown that the solutions for a steady state transition layer, discussed in Section 4e, are entirely equivalent whether closure 13a or 13b is used, provided

$$\gamma=\beta-\alpha-\alpha\beta \quad (49)$$

where $\alpha=\Delta p/P$. In the steady state dry layer problem, $\alpha=\beta/(1+\beta)$ (Betts, 1973; Tennekes, 1973), for which (49) gives $\gamma=0$. For the subcloud layer, however, β and α may vary independently.

Here α, β and γ were determined from the data. The magnitudes of α and β were discussed in Section 5c. Table 3 also gives

$$\gamma=0.22\pm0.05$$

and a corresponding value based on virtual static energy fluxes

$$\gamma_v=0.12\pm0.03.$$

Table 4 shows that the fit to Eq. (49) is reasonable.

Acknowledgments. The descriptive part of this study of subcloud layer structure was begun by Frank J. Dugan who died in a diving accident in 1974.

This research was supported by the National Science Foundation, Global Atmospheric Research Program under Grant OCD72-01406, and both the National Science Foundation and the GATE Project Office, NOAA, under Grant OCD74-21678. The VIMHEX 1972 field experiment was also supported by the Office of Naval Research under Contract No. N0014-68A-0493-002 (Principal Investigator: Dr. H. Riehl), the Meteorological Service of the Venezuelan Air Force, and the Facilities Laboratory of the National Center for Atmospheric Research. R. Miller was responsible for the data processing and computing, P. Martin for further data reduction and S. Kuehl for typing the manuscript.

I am also grateful for helpful discussion with Dr. J. W. Deardorff.

REFERENCES

Arakawa, A., and W. Schubert, 1974: Interaction of a cumulus cloud ensemble with the large-scale environment. Part 1. *J. Atmos. Sci.*, **31**, 674–701.

Ball, F. K., 1960: Control of inversion height by surface heating. *Quart. J. Roy. Meteor. Soc.*, **86**, 483–494.

Betts, A. K., 1973: Non-precipitating cumulus convection and its parameterization. *Quart. J. Roy. Meteor. Soc.*, **99**, 178–196.

——, 1974: Reply to comment on the paper "Non-precipitating cumulus convection and its parameterization." *Quart. J. Roy. Meteor. Soc.*, **100**, 469–471.

——, 1975: Parametric interpretation of trade-wind cumulus budget studies. *J. Atmos. Sci.*, **32**, 1934–1945.

——, 1976: The thermodynamic transformation of the tropical subcloud layer by precipitation and downdrafts. *J. Atmos. Sci.*, **33**, 1008–1020.

——, F. J. Dugan and R. W. Grover, 1974: Residual errors of the VIZ radiosonde hygristor as deduced from observations of the subcloud layer structures. *Bull. Amer. Meteor. Soc.*, **55**, 1123–1125.

——, and R. D. Miller, 1975: VIMHEX-1972 rawinsonde data. Atmos. Sci. Rep. 87 pp. [Available from Department of Atmospheric Science, Colorado State University.]

Carson, D. J., 1973: The development of a dry inversion-capped convectively unstable boundary layer. *Quart. J. Roy. Meteor. Soc.*, **99**, 450–467.

Cox, S. K., 1973: Infrared heating calculations with a water vapor pressure broadened continuum. *Quart. J. Roy. Meteor. Soc.*, **99**, 669–679.

Deardorff, J. W., 1970a: Preliminary results from numerical integrations of the unstable planetary boundary layer. *J. Atmos. Sci.*, **27**, 1209–1211.

——, 1970b: Convective velocity and temperature scales for the unstable planetary boundary layer and for Rayleigh convection. *J. Atmos. Sci.*, **27**, 1211–1213.

——, 1972: Numerical investigation of neutral and unstable planetary boundary layers. *J. Atmos. Sci.*, **29**, 91–115.

——, 1974a: Three-dimensional numerical study of turbulence in an entraining mixed layer. *Bound. Layer Meteor.*, **7**, 199–226.

——, 1974b: Three-dimensional numerical study of the height and mean structure of a heated planetary boundary layer. *Bound. Layer Meteor.*, **7**, 81–106.

——, E. G. Willis, and D. K. Lilly, 1969: Laboratory investigation of the non-steady penetrative convection. *J. Fluid Mech.*, **35**, 7–32.

——, *et al.* 1974: Comment on the paper by A. K. Betts "Non-precipitating cumulus convection and its parameterization." *Quart. J. Roy. Meteor. Soc.*, **100**, 122–123.

Dugan, F. J., 1973: The thermodynamic structure of the cumulus subcloud layer. Atmos. Sci. Pap. No. 205. [Available from the Department of Atmospheric Science, Colorado State University.]

Esbensen, S., 1975: An analysis of subcloud-layer heat and moisture budgets in the western Atlantic trades. *J. Atmos. Sci.*, **32**, 1921–1923.

Friedman, M., 1972: A new radiosonde case: The problem and the solution. *Bull. Amer. Meteor. Soc.*, **53**, 884–887.

Hoeber, H., 1973: The boundary-layer subprogramme for GATE. GATE Rep. No. 13., Geneva, ICSU, WMO, 132 pp.

Kraus, E. B., and J. S. Turner, 1967: A one-dimensional model of the seasonal thermocline. II. The general theory and its consequences. *Tellus*, **19**, 98–105.

Lemone, M. A., and W. T. Pennell, 1976: The relationship of tradewind cumulus distribution to subcloud layer fluxes and structure. *Mon. Wea. Rev.*, **104**, 524–539.

Lilly, D. K., 1968: Models of cloud-topped mixed layers under a strong inversion. *Quart. J. Roy. Meteor. Soc.*, **94**, 292–309.

Mahrt, L., 1976: Mixed layer moisture structure. To be published in *Mon. Wea. Rev.*

Manabe, S., and R. F. Strickler, 1964: On the thermal equilibrium of the atmosphere with convective adjustment. *J. Atmos. Sci.*, **21**, 361–385.

Nitta, T., and S. Esbensen, 1975: Heat and moisture budgets using BOMEX data. *Mon. Wea. Rev.*, **102**, 17–28.

Ogura, Y., and H. R. Cho, 1973: Diagnostic determination of cumulus cloud populations from observed large-scale variables. *J. Atmos. Sci.*, **30**, 1276–1286.

——, and H. R. Cho, 1974: On the interaction between the subcloud and cloud layers in tropical regions. *J. Atmos. Sci.*, **31**, 1850–1859.

Pennell, W. T., and M. A. Lemone, 1974: An experimental study of turbulence structure in the fair-weather trade wind boundary layer. *J. Atmos. Sci.*, **31**, 1308–1323.

Riehl, H., and A. K. Betts, 1972: Humidity observations with the 1972 U. S. radiosonde instrument. *Bull. Amer. Meteor. Soc.*, **52**, 877–878.

Sarachik, E. S., 1974: The tropical mixed layer and cumulus parameterization. *J. Atmos. Sci.*, **31**, 2225–2230.

Stull, R. B., 1973: Inversion rise model based on penetrative convection. *J. Atmos. Sci.*, **30**, 1092–1099.

Tennekes, H., 1973: A model for the dynamics of the inversion above a convective boundary layer. *J. Atmos. Sci.*, **30**, 558–567.

——, 1975: Reply to comments on "A model for the dynamics of the inversion above a convective boundary layer." *J. Atmos. Sci.*, **32**, 992–995.

Warner, J., 1972: The structure and intensity of turbulence in air over the sea. *Quart. J. Roy. Meteor. Soc.*, **98**, 175–186.

Williams, S. L., and D. T. Acheson, 1976: Thermal time constants of United States GATE radiosonde sensors. Unpubl. manuscript, CEDDA, NOAA, Page Bldg. No. 2, Whitehaven Street, Washington, D. C. 20235.

Willis, G. E., and J. W. Deardorff, 1974: A laboratory model of the unstable planetary boundary layer. *J. Atmos. Sci.* **31**, 1297–1307.

Yanai, M., S. Esbensen and J. Chu, 1973: Determination of bulk properties of tropical cloud clusters from large-scale heat and moisture budgets. *J. Atmos. Sci.*, **30**, 611–627.

Zilitinkevich, S. S., 1975: Comments on "A model for the dynamics of the inversion above a convective boundary layer." *J. Atmos. Sci.*, **32**, 991–992.